An Investigation of How Powerful a Nuclear Reactor Can Be

by

Tammy L. Stoops

Submitted to the Department of Nuclear Engineering in partial fulfillment of the requirements for the degrees of

Bachelor of Science in Nuclear Engineering
and
Master of Science in Nuclear Engineering

at the

MASSACHUSETTS INSTITUTE OF TECHNOLOGY

June 1996

Author .....
Department of Nuclear Engineering
May 10, 1996

Certified by ..
Michael W. Golay
Professor of Nuclear Engineering
Thesis Supervisor

Certified by .....
Jefferson W. Tester
Professor of Chemical Engineering
Thesis Reader

Certified by .....
Michael J. Driscoll
Professor Emeritus of Nuclear Engineering
Thesis Reader

Accepted by .....
Jeffrey P. Freidberg
Chairman, Departmental Committee on Graduate Students

An Investigation of How Powerful a Nuclear Reactor Can Be

by

Tammy L. Stoops

Submitted to the Department of Nuclear Engineering on May 10, 1996, in partial fulfillment of the requirements for the degrees of Bachelor of Science in Nuclear Engineering and Master of Science in Nuclear Engineering

Abstract

Nuclear power technologies, emitting no greenhouse gases, may be used to mitigate global warming by replacing fossil fuel energy sources. Current versions of this technology are not well-suited for this purpose, however. In order to create a suitable nuclear power system, an investigation was performed to identify and improve upon a breeder reactor system capable of large-scale power production. The system would be required to produce hydrogen as a transportable energy source, actively reduce its fission product inventory during operation, and resist nuclear proliferation.

An examination of solid, gaseous, and liquid fuel reactors indicated that the molten salt breeder reactor was most capable of meeting future needs. The development of advanced alloys is expected to reduce the problem of corrosion of the structural materials. The coating of the reactor graphite with pyrolytics or silicon carbide and the sizing of the flow channels maximize the graphite moderator lifetime. Also, chemical processing systems have been developed which appear to be adequate for the removal of the fission products, however lack of funding halted their refinement and industrial implementation.

The latest designs of molten salt breeder reactors require improvement. The chemical processing system may be simplified to a one-step, metal transfer process for fission product removal, significantly reducing the residual reactor decay power. The use of a helium-based gas turbine system eliminates hazardous interactions between the fuel and coolant. By elevating the primary heat exchanger, natural circulation may be induced to ease the cooling burden of pump failure. The decay heat can be removed using specially designed cooling tanks which allow both radiative heat losses and natural convection of air over the fuel salt. The questions of economic performance are not considered in the work reported here.

The results of this investigation show that this molten salt breeder reactor concept is passively safe. The reactor power may be increased without bound, provided that an increase is made in reactor fuel salt volume, thereby reducing the decay power density. The ability of this concept to meet the desired characteristics for a global warming response is very powerful.

Thesis Supervisor: Michael W. Golay
Title: Professor of Nuclear Engineering

Acknowledgments

I would like to thank the many individuals who provided the guidance for this project. Without the patience and advice of Professors Michael W. Golay, Michael J. Driscoll, Larry M. Lidsky, and Jefferson W. Tester, this work would never have become a reality. Without the soothing words of my fiance, Lee Carson, in times of difficulty, I would never have seen the light. I would like to extend a special thanks to Uri Gat, Kazuo Furukawa, and Dick Engel. Their genuine interest and willingness to share their invaluable experience even under the extreme conditions of a hospital stay were greatly appreciated. I truly stand on the shoulders of giants as I reach for a higher star.

I would also like to thank my mother, Anne Stoops. Despite the numerous setbacks, you have helped me maintain my hope and determination. Your confidence in me was an endless source of encouragement. As I worked diligently in a field dominated by men, your influence reminded me to never forget who I am, a woman. I love you, Mom. Thank you.

Finally, I would like to dedicate this work to my father, Richard Stoops. You have always seen the best in me, Dad, and gave me the faith to believe in myself. Because of you, I strove to reach seemingly unreachable goals and succeeded. When I stumbled, you were always there to pick me up, brush me off, and put me back on track. You have made me who I am, and taught me to acknowledge and accept what I am not. I love you, Dad. Thank you.

Contents

1 Introduction 13
1.1 General 13
1.2 Background 14
1.3 Method of Investigation 16
1.4 Scope of the Work Reported Here 17
2 Required Technology and Reactor Concepts 19
2.1 General 19
2.1.1 Large-Scale Breeding Capability 19
2.1.2 Hydrogen Production Capability 19
2.1.3 Reduction of the Core Fission Product Inventory 20
2.1.4 Nuclear Proliferation Resistance 20
2.2 Solid Fuel Reactors 22
2.3 Fluid Fuel Reactors 24
2.3.1 Gaseous Fuel 25
2.3.2 Liquid Fuel 25
2.4 Choice of Technology 27
3 Status of Molten Salt Reactor Development 29
3.1 General 29
3.2 The Fuel Cycle and Reactor Physics 29
3.3 Fuel Chemistry 31
3.3.1 Interactions of the Base Fuel Salt 31
3.3.2 Fission Product Distribution 33
3.4 Selection of Salt Container and Piping Materials 34
3.5 Graphite 36
3.6 Cooling 39
3.7 Fuel Processing 40
3.8 Required Improvements 47
4 Chemical Processing 49
4.1 General 49
4.2 One Step Processing 49
4.3 Process Efficiency and Cycle Time 50
4.4 The Fuel Decay Heat 51
5 Heat Transfer Performance 57
5.1 General 57
5.2 LiF-BeF_2, Helium, and Gas Turbines 58
5.3 Natural Circulation of the Fuel Upon Pump Failure 59

5.3.1 The Core 61
5.3.2 The Primary Heat Exchanger 61
5.3.3 The Pump 61
5.4 Natural Convection Cooling of Drained Fuel Salt 64
5.4.1 Geometry 64
5.4.2 Calculation of the Fuel Temperature 66
5.4.3 Results 67
5.4.4 Enhancement of Cooling Capacity Using Heat Storage 67
5.4.5 Toxic Effluents 75
5.4.6 Reactor Power Limitations 76
6 Further Work 77
7 Review and Conclusions 79
Appendix A: The Oak Ridge National Laboratory Molten Salt Breeder Reactor (MSBR) 83
Appendix B: Model Derivation for Natural Circulation in the Event of Pump Failure 87
B.1 Introduction 87
B.2 Conservation of Momentum 87
B.3 Heat Balance 91
Appendix C: Model Derivation for the Natural Convection Cooling of the Drained Fuel Salt 97
C.1 Introduction 97
C.2 Air Mass Flow Rate 97
C.3 Fuel Temperature 100
Appendix D: Use of Initially Solid Salt in the Natural Convection Cooling of the Drained Fuel Salt 105
D.1 Introduction 105
D.2 The Salt Temperature 105
Appendix E: Nomenclature 109
References 113

List of Tables

Table 3.1: Chemical Composition of Hastelloy N 32
Table 3.2: Fission Product Distribution for MSRE 34
Table 3.3: Chemical Composition of HN80MTY 37
Table 5.1: Natural Circulation System Parameters Required to Avoid Fission Product Volatilization 63
Table 5.2: Parameters of an Example Air Natural Convection Cooling System as Applied to the Molten Salt Breeder Reactor Reference Design 68
Table 5.3: Parameters of the Air-Natural Convection Cooling System Using an Initially Solid Salt Heat Sink as Applied to the Molten Salt Breeder Reactor Reference Design 75
Table A.1: Characteristics of the 1000 MWe MSBR 84
Table A.2: Primary Heat Exchanger Design Data 85
Table B.1: Form Loss Coefficients 89
Table B.2: The Half Lives of the 6 Representative Delayed Neutron Precursor Groups 92
Table E.1: Nomenclature 109

List of Figures

Figure 3.1: Distribution Coefficient Data Between Fuel Salt and Bismuth 42
Figure 3.2: Flowsheet for Isolation of Uranium and Protactinium by Fluorination-Reductive Extraction 44
Figure 3.3: Metal Transfer Process for Removal of Rare Earths Illustrated with Two Stages, Any Number of Stages Possible In Order to Increase System Efficiency 45
Figure 3.4: Distribution Coefficient Data Between Lithium Chloride and Bismuth 46
Figure 4.1: Comparison of Fission Product Decay Power With and Without Chemical Processing, Curves Shown for Different Processing Times 55
Figure 5.1: A Schematic Diagram of an Example Natural Circulation Configuration with Elevation of the Heat Removal Systems to Drive a Naturally Circulating Flow and a Tube Bank which Allows for Heat Rejection in the Event of Primary Heat Exchanger Failure 60
Figure 5.2: Bypassing of the Failed Pump 62
Figure 5.3: Schematic Diagram of a System for Reducing Density of Fuel Salt in the Power Plant Hot Leg by the Insertion of Helium Gas In Order to Drive a Naturally Circulating Flow for Reactor Cooling 65
Figure 5.4: Side Section View of an Example Geometry of a System for Air Cooling of the Drained Fuel Salt by Natural Convection 66
Figure 5.5: Temperature Profile Through the Fuel Salt 69
Figure 5.6: Side Section View of the Use of Initially Solid Salt in the Natural Convection Cooling System 70
Figure 5.7: Temperature Profile through the Depth of the Fuel Salt and Non-fissile Salt in the Shallow Tank as a Function of Time 71
Figure 5.8: Salt Temperature at Various Distances from the Bottom of the Shallow Tank as a Function of Time 72
Figure 5.9: Temperature Profile through the Depth of the Fuel Salt and Non-fissile Salt in the Deep Tank as a Function of Time 73
Figure 5.10: Salt Temperature at Various Distances from the Bottom of the Deep Tank as a Function of Time 74
Figure A.1: A Schematic of the MSBR 83

Figure B.1: Schematic Diagram of the Natural Circulation Primary System Geometry Analyzed in the Work Reported Here, Dimensions Labelled 88
Figure C.1: Schematic Diagram of the Geometry of the Natural Convection Cooling Tanks Analyzed in the Work Reported Here, Dimensions Labelled 98
Figure C.2: The Nodal Breakdown of the Fuel Salt 101
Figure D.1: Nodal Breakdown of the Fuel Salt and Initially Solid Salt 106

Chapter 1

Introduction

1.1 General

It has been recently suggested that nuclear technologies have a potential to mitigate global warming. Evidence suggests that human activity is changing the global climate [1]. One of the primary agents of this change is the generation of energy by burning fossil fuels. Therefore, the use of nuclear technologies may help to abate the detrimental effects of electric power production on the environment. The work reported here was undertaken in order to identify ways to modify and augment the available nuclear technology, resulting in an energy source well suited to carry society into the future.

Currently, fossil fuels provide over three-quarters of the world's energy needs. As these fuels are consumed, carbon dioxide, a greenhouse gas, is emitted. It is feared that these emissions may overheat the globe, conceivably leading to disastrous results [2]. This is becoming a growing concern as developing countries employ oil, gas, and coal in rapidly increasing quantities to meet their growing energy demands.

Numerous studies have been conducted to estimate the magnitude of the growing energy demands associated with population growth and technological advancement. An example analysis has considered the case that the world energy economy will rise from 17% to 60% of the United States per capita consumption by the year 2020 [3]. Producing no harmful greenhouse gases, nuclear power currently provides 17% of today's electricity. By utilizing nuclear power sources, geothermal sources, solar sources, or biomass sources in the place of fossil fuels, greenhouse gas emissions can be reduced significantly. The maximum benefit may only be realized, however, if one of these alternatives provides all

of the electricity consumed. The option of nuclear power is considered in the work reported here.

Electricity is not the only end product of energy generation which must be considered. The transportation industry currently consumes approximately half of the world's oil supply, contributing to carbon dioxide emissions [2]. In order to yield the maximum benefit, an alternative to fossil fuels must be applied to the transportation industry as well.

The nuclear technologies which are currently receiving the greatest developmental emphasis are passively safe and advanced evolutionary light water reactor concepts. Although these concepts are advancing the nuclear power technology base, they are ill-suited for a serious global warming response [3]. The desirable characteristics of large-scale energy production, fuel breeding, and nuclear proliferation do not exist in these proposed designs.

The purpose of this work is to provide some improvements to the current technology by applying passively safe systems to a breeder reactor which is resistant to nuclear proliferation. Improvement of the existing component systems can further augment reactor performance and safety. Hopefully enhanced performance and safety coupled with the potential for mitigation of global warming will make the proposed design of considerable interest.

1.2 Background

Ultimately, it will be necessary for nuclear power to supply much of the world's energy. Nuclear technologies are capable of both substantial short- and medium-term energy production. The world's supplies of uranium, regardless of their size, are ultimately limited in quantity. Therefore, large-capacity breeder reactor technologies would be required within several decades were nuclear power to be used in a serious global warming mitiga-

tion effort [3].

These large-scale breeder reactors would be needed to supply the energy for locations at all extents of the globe, including developing countries. These technologically primitive areas have historically had difficulties in mastering technologies which are far less demanding than those used in nuclear applications. Therefore, the probability of human error is greater in these locations. Furthermore, past experience has shown that nuclear technology is unforgiving to those who use it carelessly. It is of the utmost importance that the operators of the large-scale breeder belong to a profound "safety culture." To simply address this problem, it has been proposed that an alternate transportable energy source such as hydrogen be produced via nuclear energy. Under this proposal, hydrogen may be produced in technologically advanced regions for shipment to technologically primitive areas [3]. In addition, the hydrogen may be used to replace oil in the transportation industry. A hydrogen fuel cell also has the potential of providing electric energy silently while emitting only steam and water [2]. The safe storage, transport, and consumption of hydrogen has been accomplished in industry, however further work must be done to extend these practices to mass consumption.

Safety is yet another concern in the development of the future nuclear power technology. The primary factors affecting the nuclear hazard of a reactor must be minimized if safety is not to be compromised. Several techniques have been identified which may enhance nuclear safety. These include the following:

- A change in the configuration of the core
- A reduction in the amount of fission products in the core which produce residual heat after reactor shutdown
- An application of the hazard sharing principle with use of an on-line partial processing system [4]

In the past, the absence of these features has limited the size of reactors. It is therefore desirable to incorporate these new approaches into the design of the large-scale breeder.

Finally, the possibility of the production of nuclear weapons materials has been linked to the implementation of ostensibly peaceful nuclear power programs. A requirement for broad use is that nuclear power must not facilitate nuclear weapons proliferation [2]. Also, in order to gain social acceptance for global application, the proposed reactor must be seen to be resistant to nuclear proliferation. This may be accomplished by a number of methods including use of the U-Th fuel cycle with the newly bred fuel being continually left in the reactor system or the packaging of high intensity gamma-emitters with fuel shipments. These methods are further discussed in Section 2.1.4.

The considerations in the design of the future generation of nuclear power plants which have been mentioned here dictate their required characteristics. In summary, these characteristics include the following:

- Large-scale breeding capacity
- Hydrogen production capability
- Reduction of the fission products in the core by a hazard sharing partial processing system
- Weapons proliferation resistance.

1.3 Method of Investigation

This investigation reported here consisted of two primary tasks. The first task was the determination of the base design of a reactor which fits most readily to the characteristics required for the mitigation of global warming. This included a literature search of existing nuclear power technologies and an assessment of their respective potential for compliance with the required characteristics. In addition, concepts which had not been previously considered were examined for their feasibility.

The second task was to identify the shortcomings which are present in the current developmental stage of the base reactor design and the potential risks associated with the

operation of the plant. Features which improve upon shortcomings are proposed and evaluated. Procedures for minimizing potential risks are developed.

1.4 Scope of the Work Reported Here

The work reported here focussed primarily upon the factors which would limit the size of the power plant, improve the safety characteristics, and affect the potential use of this reactor design in a global warming mitigation effort. The economics of the design were not considered in our work. It is well-accepted that society will not adopt a new energy generation scheme if the energy produced costs more than that from fossil fuels [2]. This may be true in the short-term, but the future of our planet may require that alternate power production methods be utilized in order to reduce the change that we humans may inflict upon the earth's climate and ecosystems. We expect that if this power production method were to replace all of the current power technologies, a new market would be created and any economic analysis completed at the time of this writing would be irrelevant.

Chapter 2

Required Technology and Reactor Concepts

2.1 General

The breadth of nuclear power technology was considered in our determination of the base reactor concept which would be most capable of possessing the required characteristics for the mitigation of global warming. As identified in Section 1.2, the ideal energy generation system would possess a large-scale breeding capacity, hydrogen production capabilities, partial processing of the fuel for the reduction of fission product inventories, and proliferation resistance. There are several ways which each of these requirements may be attained.

2.1.1 Large-Scale Breeding Capability

Net production of fissile nuclei, or breeding, in the reactor core is a direct function of the physics of the chain reaction. The possibility for breeding exists when the average number of neutrons produced per neutron absorbed in the fuel, known as the parameter η, is greater than 2. Both thermal and fast reactor systems may use the excess neutrons to produce more fissile material. ^{233}U has the largest η value for a thermal neutron spectrum, providing the ^{232}Th-^{233}U fuel cycle with the highest potential for breeding in a thermal reactor. In a fast neutron spectrum, the transmutation of ^{238}U to the ^{239}Pu and ^{241}Pu isotopes shows the most promise [5].

2.1.2 Hydrogen Production Capability

A number of methods exist for the production of hydrogen. Based on the status of current technologies, the most attractive means is electrolytic. Alternate means include thermally- and chemically-based methods, however neither of these have been developed to the stage of industrial application as of this writing [6].

2.1.3 Reduction of the Core Fission Product Inventory

A reduction in the concentration of fission products in the core has proven to be a tremendous technological challenge. Most developmental efforts toward the on-line partial processing suggested by Lidsky have been halted by economic factors [4]. Designers of processing systems were aiming to compete economically with light water reactors. Unable to achieve this goal before governmental funding of the projects was terminated, the application of chemical processing systems to nuclear power technology was never realized. As mentioned earlier, the economics of the system are beyond the scope of this investigation and, therefore, will not eliminate the requirement of a processing system for the reactor design of choice.

By removing a fraction of the fission products from the reactor during operation, the amount of residual heat which must be removed from the fuel after reactor shutdown is decreased. Rather, these fission products would be heating the fuel wastes which also must be cooled, however this cooling would be performed on a routine basis in a separate facility. This results in a much safer reactor system. Previous efforts to develop a very safe reactor have yielded much smaller units such as the modular high temperature gas-cooled reactor (MHTGR) concept. These units are not suited to supply the world energy economy. Therefore, a partial processing system is a desirable element of future nuclear power plants.

The fission product removal capability may be facilitated only if the fission products may be separated from the fuel in which they originate. This separation could arise from either the migration of fission products from a solid fuel (probably in a small pellet geometry) or physical separation from a fluid fuel.

2.1.4 Nuclear Proliferation Resistance

The societal acceptance of the nuclear power program depends upon the implications

which the system would have on the manufacturing of nuclear weapons. Although no system may guarantee an end to the threat of nuclear warfare, some systems are capable of a greater deterrence to weapons production. Two aspects of such systems are the utilization of the uranium-thorium fuel cycle and the packaging of high energy gamma-emitters with fuel shipments. Of all potential fuel systems, ^{233}U is the least desirable material for the construction of a nuclear weapons arsenal due to the ease with which other fuels may be transformed into weapons grade material. In the event that this material were to be used for bomb construction, the manufacturer would be deterred by the risk associated with the handling of ^{233}U. In a reactor which consumes a ^{233}U fuel, ^{232}U will be generated at a concentration of approximately 500 ppm. ^{208}Te, a daughter product of ^{232}U (being produced by activation of ^{232}Th), emits 2.6 MeV gamma rays. At 0.5 m from 10 kg of an unshielded ^{233}U fuel element, an individual will receive an estimated radiation dose of 200 rem/hr, a dose which will prove to be lethal in a two hour exposure time [7]. This same concept may be applied to fuels which do not inherently possess this proliferation resistance tactic by packaging the fuel shipments with high intensity gamma-emitters [3].

These methods address the problem of diversion of nuclear materials which are not contained in the reactor. For reactor systems with on-line chemical processing, the only material removed from the primary system is the fission products. The fissile isotope remains in the fuel in the reactor from the time which it was bred until the time which it is consumed. Without leaving the reactor, the possibility for diversion of the fissile material is significantly reduced.

Beginning with these proposed methods for satisfying the requirements of large-scale breeding capacity, hydrogen production capability, core fission product concentration reduction, and nuclear proliferation resistance, the nuclear power technologies were evaluated for their feasibility. This feasibility evaluation involved a literature search to deter-

mine the present status of each technology coupled with an evaluation of some creative new concepts. The technologies considered may be categorized as solid or fluid fuel concepts.

2.2 Solid Fuel Reactors

To this date, engineers have devoted the majority of their resources to solid fuel technologies, as evidenced by the massive volume of technical literature on the subject [5, 8, 9]. Of particular interest are the large-scale breeding reactors in compliance with the first requirement for global warming mitigation. Solid fuel experience has produced reactors designs with both thermal and fast neutron spectrums. In 1982, the United States Department of Energy's Light Water Breeder Reactor (LWBR) project confirmed breeding using uranium-thorium fuel at the Shippingport nuclear power station. In December of 1986, the first commercial-sized liquid metal fast breeder reactor (LMFBR), the Superphenix, reached full power, proving the possibility of large-scale breeding in a fast reactor system [5].

Although the operation of these reactors has provided a wealth of valuable knowledge and information regarding large-scale breeding using solid fuel, neither system was capable of substantially reducing the core's fission product content. A reduction of the core fission product concentration in reactors of this category would rely upon the diffusion of the fission products out of the solid fuel.

The removal of fission products which have migrated out of the fuel region may be facilitated in an uncladded core design. By removing the cladding, the coolant makes direct contact with the fuel and carries away the fission products. The fission products are then removed from the coolant in an on-line processing plant. In order for this concept to work, the fission products must be capable of migrating out of the solid fuel to the coolant.

The size of the solid fuel particles will dictate the success of fission product escape from the core. Therefore, it is most desirable to size the fuel particles with this in mind.

Fission product migration from the site of a fission reaction is enabled by the temperature gradient which exists across the fuel cross section. The extent and mechanism of the migration is a function of the particular species of fission product. Zirconium, niobium, yttrium, and the rare earths, important because of their decay heat contribution, have experimentally shown little migration in uranium oxide fuels [8]. Not relying of migration, a fission product may escape the fuel only before it loses the kinetic energy imparted to it by the fission process. This is possible if the initial energy imparted to the particle by the fission process will carry it beyond the extent of the fuel.

The nuclear mass distribution of fission products readily lends itself to the classification of fission products as heavy or light nuclei. Each nucleus is generated with approximately half of the number of electrons present in the uncharged isotope. Through a series of ionizing collisions, the heavy and light fission products are brought down from initial energies of approximately 63 meV and 95 meV respectively to being in thermal equilibrium with the fuel medium. In air, the typical ranges for the heavy and light fission products are 20 mm and 25 mm respectively [10]. In order to ensure removal of all fission products, the fuel size must be less than the range of the heavy isotopes. The range in uranium may be estimated from the range in air using the following correlation [11]:

$$\frac{R_U}{R_{air}} \approx \frac{\rho_{air}\sqrt{A_U}}{\rho_U\sqrt{A_{air}}}. \tag{2.1}$$

This yields a range of 0.48 micron in solid uranium. If the density of the uranium is decreased by employing a sponge-like material, the range is approximately 1 micron. These conditions may be satisfied by a fluidized bed of porous uranium particles approximately 1 micron in diameter.

With the size of the fuel particles determined, a coolant must be chosen. Utilizing the uranium-plutonium fuel cycle due to the greater amount of experience with these fuels, a non-moderating coolant is required. Molten lead shows promise with the potential of a direct contact steam generator which would maximize thermodynamic efficiency.

As the molten lead circulates through the core region, the fuel particles must be confined to this region without being carried away by the coolant. This condition will be met only if the weight of a particle is greater than the aerodynamic drag of the coolant. The drag may be determined by the following relation:

$$D = \frac{1}{2} C_D \rho v^2 A, \tag{2.2}$$

where D is the drag force, C_D is the coefficient of drag, ρ is the fluid density, v is the fluid velocity, and A is the projected area of the fuel particle. The values of the coefficient of drag are a function of the Reynolds number of the flow past the fuel particle [12]. With a fuel particle 1 micron in diameter, the fluid velocity must remain less than 3×10^{-6} m/s in order to avoid fuel particle escape from the core region.

This particular core design has become, in effect, a homogeneous liquid in order to satisfy the requirement of fission product removal. The low coolant velocities which are needed to restrict the fuel particles to the core region are impractical. Therefore, we focus attention upon fluid fuel reactors, which do not restrict the fuel to the core region.

2.3 Fluid Fuel Reactors

Proposed designs for fluid fuel reactors generally circulate the fuel which may be either gaseous or liquid in nature. This behavior provides a number of advantages over their solid fuel counterparts such as a simpler reactor core configuration, easy handling of the fuel, easy processing of the fuel, and potentially simple, safe operation. Accompanying

these advantages are a number of disadvantages which include material compatibility problems, possible fluctuations in reactivity caused by changes in fuel concentration or density, and loss of delayed neutrons in the fuel leaving the core [13]. Research has attempted to overcome these obstacles with the development of both gaseous and liquid fuel reactors.

2.3.1 Gaseous Fuel

A number of varying concepts have been suggested for the use of gaseous fueled reactors. The experience with the gaseous diffusion techniques employed in the enrichment of uranium may be applied to this reactor type in order to remove the fission products from the fuel stream, making gaseous fuel an attractive choice. The core configuration varies dramatically from the traditional solid fuel reactor with either a highly pressurized cavity or a graphite moderating block with flow channels for the fuel. In the cavity reactors, extreme operating conditions must be maintained in order to achieve criticality. With an estimated wall temperature of 3500 K, there are no carbon compounds which may withstand the reactor environment. In addition, there is no known gaseous uranium compound which will remain stable at these elevated temperatures [14]. In order to overcome these difficulties, a gaseous uranium hexafluoride fuel may be circulated through a graphite moderating region. The power size of this reactor type is limited, however, by the enrichment of the fuel. If the enrichment is maximized, the power rating must be boosted by increasing the fuel density with a pressure increase [15]. These limitations prevent the required large-scale energy generation capability for future global warming mitigation.

2.3.2 Liquid Fuel

The final category of reactor fuels is that of liquids. Aqueous homogeneous, liquid metal, and molten salt fuel types have been used in practice, each with varying degrees of success. The aqueous homogeneous reactors circulate a slurry of uranyl sulfate and water.

These systems are typically operated at high pressures. Difficulty arises as the water begins to dissociate during operation [16]. This dissociation (hydrolysis) is caused by the ionizing radiation produced by the fission process. Particles emitted with a wavelength less than 250 angstroms and an energy greater than 50 eV have the potential to dissociate the water content of the fuel [6]. The fuel composition may also be altered in the event of an accident as the uranyl sulfate particles settle out of the slurry. As these processes alter the fuel density and concentration, the reactivity of the core fluctuates. The liquid metal and molten salt reactors resolve the issue of dissociation and separation of the fuel. Prototypes of this nature have experienced rapid corrosion of their container materials, however [13]. Materials scientists have had the greatest degree of success in the development of new materials for the molten salt reactor, enabling the possibility of future commercial utilization of the molten salt reactor.

The bulk of research and development efforts dedicated to the molten salt reactor have been concentrated at the Oak Ridge National Laboratory (ORNL), with the exception of the contributions of Kazuo Furukawa [13] and Vladimir Novikov [17]. Conceptual designs employ a uranium-thorium fuel cycle, meeting the requirements of breeding capability and proliferation resistance. The U-Th neutronic behavior favors fuel breeding most if a thermal neutron spectrum is used. Requiring thermal neutrons, the fuel may only achieve criticality as it flows through a graphite moderating region. This allows the fission chain reaction to be halted by simply draining the fuel from the core. The fuel may then be directed to an alternate location where it may be configured to a geometry which maximizes the decay heat cooling capacity. A processing system was under development at ORNL which was intended to minimize the fuel doubling time and maximize fission product removal; governmental funding difficulties halted these efforts. Current proposals, such as the FUJI reactor, consist of smaller reactor systems in order to maximize the safety

which is lost with the removal of the fuel processing plant from the overall power plant complex [13]. The potential exists for the need for this processing plant to be reevaluated and improved, eliminating the need for the reduced power capacity. Coupled with modern techniques for passive cooling of the reactor fuel in a favorable configuration, the molten salt reactor may satisfy all of the characteristics of the ideal future generation of nuclear power plants.

2.4 Choice of Technology

In choosing the basis for the future generation of nuclear energy systems, the reactor designer is confronted with the options of solid, gaseous, and liquid fuels. In order for these fuels to meet the desired characteristics for the mitigation of global warming, the technologies must employ a breeding fuel cycle, have a hydrogen production capacity, process the fuel for fission product removal, and resist nuclear proliferation as they operate in a safe manner. The reactor most capable of meeting these specifications appears to be the molten salt breeder reactor.

Chapter 3

Status of Molten Salt Reactor Development

3.1 General

The use of a molten fuel salt in the nuclear technology efforts to mitigate global warming introduces a number of issues unique to fluid fuel reactors. The corrosion of container materials, interactions with extraneous materials, and fission product deposition must be carefully considered in addition to the physics, energy production, and safety of the plant. Extensive research has been performed in these areas to date.

3.2 The Fuel Cycle and Reactor Physics

Any material which is chosen for nuclear applications must remain chemically stable in the environment to which it will be subjected. This applies to the fuel consumed in the molten salt reactor. Analyses of salts which form compounds containing the elements uranium and thorium were completed in order to determine the most suitable fuel. It was found that a fluoride based salt possesses the most desirable characteristics [18].

The exact composition of the fuel salt is also dependent upon the configuration of the core. Molten salt reactor designs have been characterized as either one- or two-fluid reactor systems. In the one-fluid system, the fertile and fissile material are contained in the same salt. The graphite moderator forms both the core and blanket regions with varying densities of the graphite in each region. The two-fluid reactor system utilizes separate fissile and fertile salts, separating the two with graphite tubes. Extended operation of this configuration proved that the graphite lost integrity and leaked due to irradiation damage, allowing the salts to mix. Therefore, one-fluid systems have been adopted [18]. One-fluid molten salts contain both the fertile and fissile material. Using a fluoride base salt, a typi-

cal molten salt reactor fuel is 72% LiF, 16% BeF_2, 12% ThF_4, and 0.3% UF_4. This salt melts at a temperature of 434°C, requiring that the reactor operate in an elevated temperature range of 434°C to approximately 710°C. The stability of this fuel in irradiation environments at this elevated temperature has been demonstrated [19].

Operation of a thermal reactor system with the uranium-thorium fuel cycle results in a relatively low breeding ratio in comparison to their fast reactor counterparts. The breeding ration is defined as the ratio of the rate of creation of new fissile material to the rate of destruction of existing fissile material [5]. The calculation of the breeding ratio has yielded values in the range of 1.05 to 1.07 [18]. This calculation contains far more uncertainty than the calculations for fast systems. The breeding ratio is a function of the number of neutrons available for capture in the fertile material. This number of neutrons is given by the parameter η. Incorporating a spectrum averaged value for the ^{233}U η introduces significant uncertainty. The η value of 2.293 ± 0.01 results in an uncertainty in the breeding ratio of 0.008. This is quite significant. Further experiments must be performed to provide a more accurate value for η [19]. Regardless, the breeding ratio may be increased by holding the neutron absorbing isotope ^{233}Pa, with its 27.4 day half life, outside the core where the absence of neutron irradiation will allow this isotope to decay to ^{233}U [18].

Control of the fission process is provided to the reactor in several variable forms. For long-term control, the composition of the fluid fuel may be altered. This eliminates the need for a built-in excess reactivity to compensate for fuel burnup and the continuous neutronic poisoning caused by the accumulation of fission products. In general, thorium and fissile ^{233}U are added as fresh components as fuel is consumed and fertile material is converted into fuel [20]. For short-term control, graphite displacement rods and Gd_2O_3-Al_2O_3 ceramic absorbing rods can be employed. With this concept. the graphite rods provide a boost of positive reactivity as they displace fuel salt, partly due to the increased neutron

resonance capture in the flow channels neighboring the displaced channel. A similar effect has bee observed in natural uranium graphite reactors [19]. The Gd_2O_3-Al_2O_3 ceramic rods are hollow and cylindrical in shape. In the Molten Salt Reactor Experiment (MSRE) at ORNL, these cylinders were canned in Inconel and threaded on a stainless steel hose. The hose provided a cooling air conduit for the rod [21].

An aspect of the molten salt reactor which is not observed in its solid fuel counterparts is the effect of fuel circulation. As delayed neutrons leave the core region with the flowing fuel salt, the effective delayed neutron fraction in the core is reduced. This reduction takes the overall delayed neutron fraction of 0.0030 down to a value of 0.0017 for ^{233}U [21]. This resulted in a net negative reactivity contribution of approximately 0.222 $\delta k/k$ for the MSRE.

3.3 Fuel Chemistry

The chemistry of the molten salt reactor is constantly changing due to the generation of fission products. In order to understand the behavior of the fuel salt under all operating conditions, it is essential to consider both the interactions of the base fuel salt with the neighboring materials and the effects of the fission products on the structural materials.

3.3.1 Interactions of the Base Fuel Salt

Throughout the lifetime of the reactor, the base fuel salt will come into contact with an array of materials. The container materials, moderating graphite, air, and water are the main components whose interactions with the salt must be understood. The circulation of the fuel salt ensures that the fuel is well mixed, allowing the interactions to be characterized on a consistent basis [22].

The primary structural material for the molten salt reactor is a slightly modified alloy of Hastelloy N with low iron content. The chemical composition of Hastelloy N is shown

Table 3.1: Chemical Composition of Hastelloy N [23]

Element	Content (% by weight)	
	Standard Alloy	Favored Modified Alloy
Ni	Base	Base
Mo	15-18	11-13
Cr	6-8	6-8
Fe	5	0.1
Mn	1	0.15-0.25
Si	1	0.1
P	0.015	0.01
S	0.020	0.01
B	0.01	0.001
Ti		2
Hf		2
Nb		0-2

in Table 3.1. This material was developed especially for use with molten fluorides in the aircraft industry [18]. The major fuel components (LiF, BeF_2, ThF_4, UF_4) are much more stable than the fluorides formed with the elements present in the Hastelloy, making the salt thermodynamically stable toward the structural material [24]. Two noteworthy exceptions are chromium and titanium. These elements form fluorides more readily, and therefore it should be expected that the Cr and Ti on the surface of the Hastelloy will react with the fuel. As the structural material is heated, the Cr and Ti will migrate along the temperature gradient toward the cold regions away from the salt. Concentrating in the outer layers of the structural material, the amount of Cr and Ti available to interact with the fuel salt is reduced [22].

The moderating graphite material, on the other hand, does not react with the fuel salt. The molten salt does not have the capability to wet the graphite, and penetration will not occur if the graphite pore size is kept smaller than one micron [24].

Leakage of air or water into the primary circuit may occur, necessitating that the salt be compatible with these materials as well. The introduction of water vapor into the molten salt will produce hydrofluoric acid, a corrosive agent, and cause the actinides to precipitate out of solution. Rapid insertion of water into the system may also lead to the precipitation of uranium dioxide. These interactions may be limited by controlling the environment within the containment. Air will cause no problems with the fuel salt, but still presents corrosion difficulties. The oxidation of the metallic surfaces in the reactor system will occur if the addition of air is not controlled [24].

3.3.2 Fission Product Distribution

During normal operation, fission products will be added to the fuel fluid. These fission products may be classified as noble gases, rare earth stable salt-seeking fluorides, noble metals, and other stable salt-seeking fluorides. Each category will be distributed in a different manner in the reactor system [24]. This was illustrated with the operation of the MSRE. Table 3.2 shows the distribution of fission products at the end of MSRE operation.

The first category, the noble gases, is removed from the fuel by means of an off-gas system. The gases are stripped from the liquid salt and trapped in charcoal filters [22]. Doing this eliminates the noble gas fission product content of the fuel salt. The rare earth stable salt-seeking fluorides include Rb, Cs, Sr, Ba, Y, Zr, and the lanthanides. These elements form fluoride compounds and remain in the salt mixture. The elements Nb, Mo, Tc, Ru, Ag, Sb, and Te are classified as noble metals. They may appear in the salt, in the purge gas, on the Hastelloy N, or on the graphite. The preferential distribution may be characterized as roughly 50% in the purge gas due to bubble splashing, 40% on the metal, and 10%

Table 3.2: Fission Product Distribution for MSRE [24]

Nuclide	Quantity Found (% of Calculated Inventory)				
	In Fuel	On Graphite	On Hastelloy N	In Purge Gas	Total Observed
^{99}Mo	0.17	9.0	19	50	78
^{132}Te	0.47	5.1	9.5	74	89
^{129}Te	0.40	5.6	11.5	31	48
^{103}Ru	0.033	3.5	2.5	49	55
^{106}Ru	0.10	4.3	3.2	130	138
^{95}Nb	0.001 to 2.2	41	12	11	64
^{95}Zr	94	0.14	0.06	0.43	95
^{89}Sr	83	8.5	0.08	17	109
^{140}Ba	96	1.9	0.05	0.48	98
^{141}Ce		0.33	0.03	0.88	
^{144}Ce		0.92	0.03	2.7	
^{131}I	60	0.11	0.3	19	80

on the graphite. The deposits are generally fine, well-mixed material as opposed to plating [13].

Finally, tritium will be produced in the molten salt reactor. In operation, the tritium has tended to migrate from the fuel salt, through the secondary coolant salt, and into the tertiary water loop. In this loop, the tritium is transferred to the cover gas where it may be recovered as either H_2 or, via beta decay, elemental He [13].

3.4 Selection of Salt Container and Piping Materials

Historically, the most difficult challenge to overcome in the design of a fluid fuel reactor has been the selection of the vessel and piping material. The material must sustain the temperatures spanned in each fluid loop as well as the applied thermal stresses and chemi-

cal reactivity. Fission product deposition on structural surfaces must be tolerated. In addition, the integrity of the material under irradiation is paramount [23].

The corrosion incurred through interactions with the fuel salt or extraneous materials must be minimized. In the molten salt reactor, the primary concerns include the selective leaching of the chromium and titanium by the fluoride salt discussed in Section 3.3 and the oxidation of the internal metal surfaces in the event of an in-surge of air. Impurities in the salt may also lead to accelerated corrosion of all structural elements, requiring that the purity of the salt be continually monitored [23].

Hastelloy N constituted the structural makeup of the MSRE. The composition of this alloy is shown in Table 3.1. Because the oxidation of iron occurs more readily than that of nickel, the concentration of iron was reduced in the modified alloy. Small quantities of chromium are included to improve the oxidation resistance. For strengthening purposes, molybdenum was added [23].

As the reactor is brought into operation, the structural material is exposed to irradiation. The Hastelloy N displayed helium embrittlement comparable to that expected in non-molten salt environments. Addition of titanium, hafnium, zirconium, or niobium to the alloy increases embrittlement resistance with the formation of finely dispersed MC type carbides. The carbides trap the helium, preventing its accumulation at the grain boundaries. The neutron fluences impinging upon the structural materials were maintained at sufficiently low levels to prevent both swelling and void formation [23].

With the subjects of chromium leaching and irradiation embrittlement under control, investigation of the MSRE structure displayed evidence of intergranular cracking. The cause of this cracking was traced to the deposition of the fission product tellurium on the "cold" Hastelloy N surfaces [17]. By forming a low-melting nickel-tellurium eutectic with the segregation of tellurium in the grain boundaries, the strength of these regions was

weakened in comparison to the bulk material. A proposal from the team at ORNL suggested that the addition of chromium would slow the formation of the eutectic. Balancing the effects of increased corrosion by the fuel salt and slowed intergranular cracking, the team at ORNL proposed a modified alloy whose composition is detailed in Table 3.1 [23].

An optimization of the chromium content is not the only potential solution to the problem of intergranular cracking. The research of Novikov et. al. has yielded an alternative material, HN80MTY [17]. In attempt to improve the behavior of the modified Hastelloy N, the chromium content was reduced slightly. A reduction in the chromium content induced a deteriorated heat resistance of the material. In order to augment the heat resistance as well as decrease the intergranular cracking due to tellurium deposition, aluminum was introduced to the material with a subsequent reduction in the titanium content. Addition of the aluminum decreased and changed the character of the carbide phase formation along the grain boundaries, preventing the formation of the detrimental nickel-tellurium eutectic [17]. The resultant alloy displayed superior corrosion and intergranular cracking resistance. The composition of HN80MTY is shown in Table 3.3.

3.5 Graphite

Special consideration must be placed on the reactor graphite, even though there are no interactions between this carbon compound and the salt. The graphite has a finite lifetime and will therefore require periodic replacement. Optimal design would extend the graphite lifetime to coincide with regular steam turbine maintenance which will be required on an average interval of two to three years [25]. Conceivably the reactor could be designed to permit on-line graphite replacement, segment by segment.

Throughout the life of the reactor, the trapping of fuel salt or neutron absorbing xenon in the moderating material must be avoided. The salt is unable to penetrate pores in the

Table 3.3: Chemical Composition of HN80MTY [17]

Element	Content (% by weight)
Ni	Base
Mo	11-12
Cr	5-7
Fe	1.5
Mn	0.5
Si	<0.15
P	0.015
S	0.012
Ti	0.5-1
C	<0.4
Al	0.8-1.2

graphite of a size smaller than one micron; this is not the limiting factor, however. In order to minimize the permeation of xenon, the pore diameter must not exceed 0.1 micron [25].

In determining the initial pore size limitations, the behavior of the graphite under irradiation must be examined. The volumetric distortion of graphite is given empirically by the following parabolic relation:

$$\nu = A\Phi + B\Phi^2. \tag{3.1}$$

In this expression, ν is the volumetric expansion, Φ is the neutron fluence, and A and B are positive in sign and functions of temperature only. Upon onset of irradiation, the graphite volume begins to decrease as the vacancies in the lattice collapse. This process slows and reverses, resulting in extensive swelling during prolonged radiation periods [25]. It is during this expansion that the enlargement of the pores becomes limiting.

The behavior of the volumetric distortion is strongly dependent upon the internal temperature of the graphite. As the temperature increases, the lifetime of the graphite

decreases. This internal graphite temperature distribution is affected by the mass flow rate of the fuel salt, the salt-to-graphite ratio, and the diameter of the graphite channels. The mass flow rate of the salt is determined according to the cooling capabilities of the system and the salt-to-graphite ratio by the reactor's neutronic and criticality requirements. The diameter of the flow channels is therefore the only parameter which can be controlled to lower the internal graphite temperature. As the channel diameter increases, the graphite lifetime decreases [25].

An analysis of the internal stresses on the graphite moderator have also been completed. These analyses show that the imposed stress is an order of magnitude lower than the yield strength of the graphite [25]. Therefore the most stringent limitations are those of volumetric expansion.

A variety of graphite types have been considered for use in molten salt reactor applications. Of special interest are the monolithic materials, desired for their homogeneity and prolonged stable induction period before the inception of the expansion which follows the parabolic behavior described by equation (3.1). This time and rate dependence of this behavior is included in the neutron fluence [26]. At least one commercial graphite in this category, British Gilso graphite, is suitable for this application [27]. It has been estimated that this graphite will have a lifetime of approximately four years. Methods for the resistance to salt or xenon impregnation have also been postulated. During the heyday of molten salt reactor development in the 1960 and 70s, the use of the newly developed pyrolytics appeared to introduce the possibilities of coating or impregnating the graphite in order to increase its durability and lifetime. More recent experience with silicon carbide coatings used in pebble-bed HTGR-type reactors may be applicable to the molten salt reactor graphite as well [25].

3.6 Cooling

The energy generation of any power plant is dependent upon a reliable, efficient cooling system. In the molten salt reactor, three loops are employed. The primary circuit circulates the fuel salt, the secondary the cooling salt, and the tertiary the steam used in the power conversion system. The secondary loop containing the cooling salt provides a barrier to confine the fuel salt, transfers heat from the fuel salt to the steam, and bridges the temperature gap between these fluids [21]. With the circulation of the fluid fuel out of the core to transfer its heat to the secondary coolant through an external heat exchanger, the molten salt reactor cannot experience a loss-of-coolant accident (LOCA) [20].

The choice of the coolant salt is contingent upon its compatibility with the fuel, steam, and structural materials, its thermal properties, and its irradiation stability. In the MSRE, a LiF-BeF_2 salt was employed, operating in the temperature range of 538 to 650°C. The heat was removed from the coolant with the use of an air-cooled radiator. In the design of their molten salt breeder reactor, the team at ORNL decided to use a steam turbine system. With this choice, a restriction that the coolant salt must remain in liquid state at the lowest circulating temperatures possible for designs employing a steam system was imposed [24]. The LiF-BeF_2 coolant salt could not satisfy this criterion with adequate margin with its melting point of 455°C, and therefore an alternate mixture had to be determined.

After consideration of all available fuel salts, the secondary coolant sodium fluoroborate was selected despite the increased difficulty with chemical compatibility in comparison to the LiF-BeF_2. The NaF-$NaBF_4$ has a melting point of 385°C, requiring that the feedwater temperature not fall below 371°C in the steam generator. In order to ensure that this temperature limit will be respected, preheaters are essential in the tertiary loop [28]. At the turbine throttle conditions of 538°C, 3500 psia, a 44% overall plant efficiency was achieved [29].

The chemical compatibility of the sodium fluoroborate is of concern. In the presence of moisture, hydrofluoric acid and sodium hydroxyfluoroborate, corrosive agents, are produced. The NaF itself is chemically toxic. In addition, fluorine will be produced in the presence of radiation. As in the fuel, the secondary coolant will selectively leach the chromium and titanium in the Hastelloy N piping. When mixed with the fuel, the coolant readily dissociates producing BF_3. This BF_3 gas pressurizes the primary system. It is believed by the team at ORNL that this will not be a problem as the production of the gas will be slowed by the immiscibility of the coolant in the fuel salt [28]. With the potential for stress corrosion cracking of the steam generator tubes, it becomes essential that duplex tubes be utilized. Though these difficulties have been identified, the team at ORNL was under the belief that they do not provide an insurmountable barrier to the use of steam turbines.

3.7 Fuel Processing

The removal of fission products from the fuel for the reduction of the decay heat load is done through use of a chemical processing system. Utilizing this processing system, the reactor is operated at an equilibrium steady state. The concept of burnup has no meaning as the fuel fissile isotope concentration and content do not vary with time and there exists no fuel crystalline structure to be damaged by radiation [20]. For the molten salt breeder reactor, an additional requirement is that the protactinium produced from neutron absorptions in ^{232}Th must be shielded from the neutron flux in order to allow increased quantities of the protactinium to escape the possible neutron absorption and decay to ^{233}U. If the protactinium were to absorb a neutron, ^{234}U, a parasitic neutron absorber, would be produced by the beta decay of ^{234}Pa. Research at ORNL presented a processing system which would meet these requirements, however the funding associated with the ORNL system

and its economic competitiveness with light water reactors have halted its progress [13].

The first step in the removal of the fission products is the transfer of the gaseous fission products such as xenon and krypton from the fuel salt to the off-gas system. Although the bulk of the gas escapes the salt, small quantities remained trapped. In order to facilitate the removal of the remaining gas, helium may be bubbled through the salt, providing a means of escape [25].

Next, the protactinium is removed from the fuel for storage. The process for the protactinium removal consists of concurrently contacting the fuel stream with a bismuth stream which contains small quantities of lithium. The bismuth dissolves metallic Li, Pa, U, Th, and the rare-earths to varying extents. The reductive extraction reaction between materials in the salt and metal phases may be represented by the following:

$$MF_n\,(salt) + nLi\,(Bi) \Leftrightarrow M\,(Bi) + nLiF\,(salt) \tag{3.2}$$

The extent of the separation is given by the distribution coefficient, D. D is defined as the ratio of the mole fraction of M in the metal bismuth phase to the mole fraction of MF_n in the salt phase where M is the respective metal. The data for the distribution between the fuel salt and bismuth are illustrated in Figure 3.1. The ease of separation of the components from the salt phase is indicated by the ratio of the respective distribution coefficients. The distribution coefficients vary enough to enable the separation of the protactinium, however the uranium will distribute in a manner similar to the protactinium causing the removal of this fissile isotope as well [30].

In order to circumvent the removal of the uranium with the protactinium, it has been proposed that the uranium be removed from the fuel salt phase prior to its countercurrent contact with the bismuth phase. Uranium removal may be accomplished by fluorination of the fuel salt. This method has been proven with the processing of batches of the fuel salt,

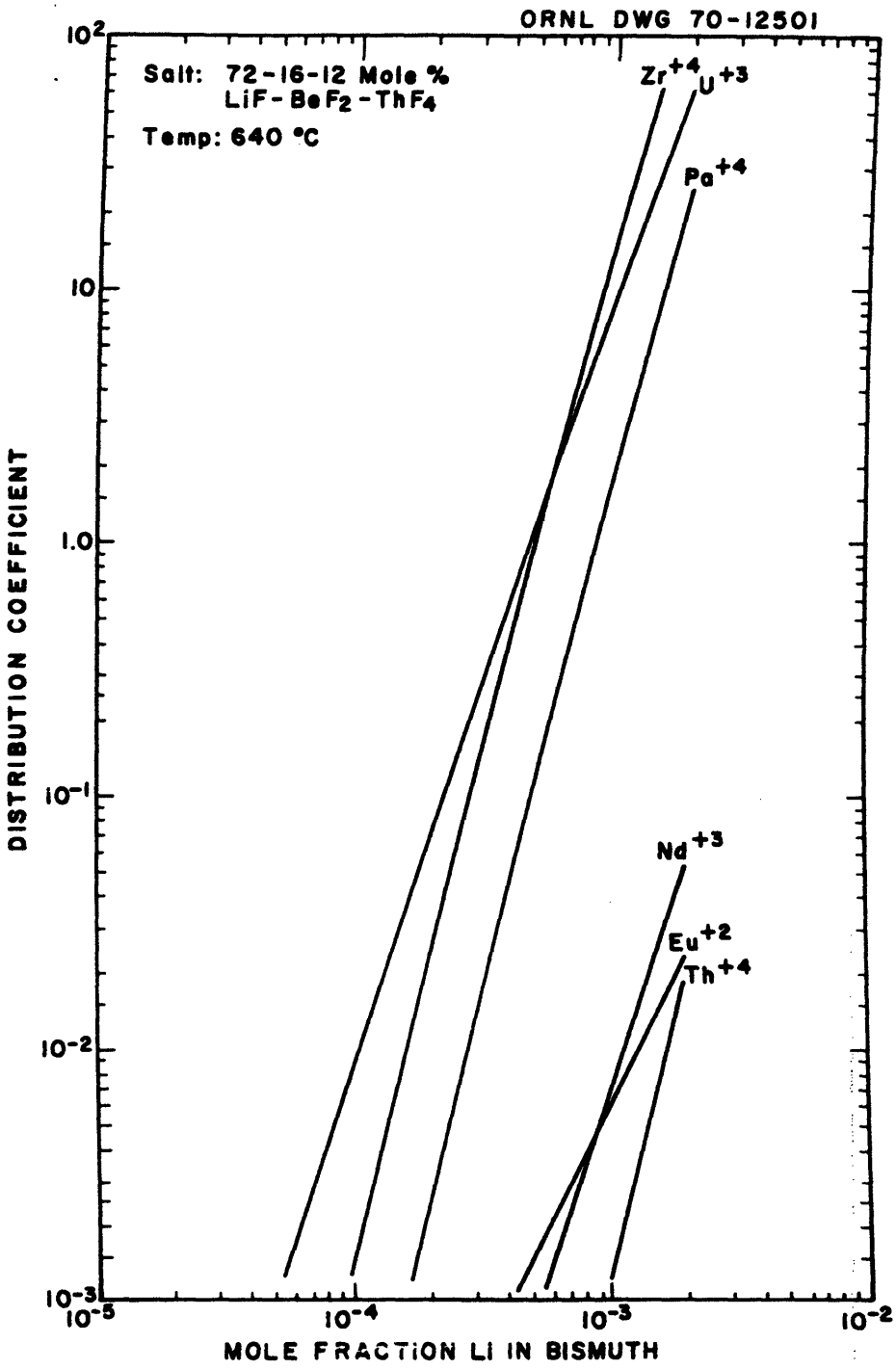

Figure 3.1: Distribution Coefficient Data Between Fuel Salt and Bismuth [30]

however extreme difficulties have arisen in the development of continuous fluorinators suitable for on-line molten salt processing [31]. A flowsheet illustrating the removal processes for both the uranium and protactinium is shown in Figure 3.2.

Once the protactinium has been removed, the remaining fission products must be gleaned from the salt. From Figure 3.1, it may be seen that the distribution coefficient of thorium and the rare-earths are approximately equal, requiring a different process to be used for fission product isolation. The process which is most capable of rare-earth removal consists of concurrently contacting the fuel salt with a bismuth stream which is then countercurrently contacted with a lithium chloride stream. This scheme is illustrated in Figure 3.3 with two stages. The number of stages may be increased to any number of stages in order to achieve the desired separation efficiency. The distribution coefficients, shown in Figure 3.4, allow the separation of the rare-earths from the fuel stream [30]. Upon removal of the rare-earths, the fuel must be reconstituted. Preliminary studies have shown that the absorption of UF_6 by the fuel salt is slow. Further development efforts are required in this area.

The use of bismuth as a reductant in the processing plant introduces a complication. As the fuel is concurrently contacted with the bismuth, bismuth is entrained and, to a much lesser degree, dissolved in the fuel salt. Nickel is quite soluble in liquid bismuth at plant operating temperatures, requiring that all bismuth be removed from the fuel salt. This may be done by contacting the fuel salt with a large surface area of nickel provided by nickel wool before it is returned to the coolant loop. An alternative to the removal of the bismuth from the salt phase is the protection of the structural materials from direct contact with the fuel salt. Development efforts have produced pipes lined with solid fuel salt, minimizing the direct contact of nickel and bismuth [30].

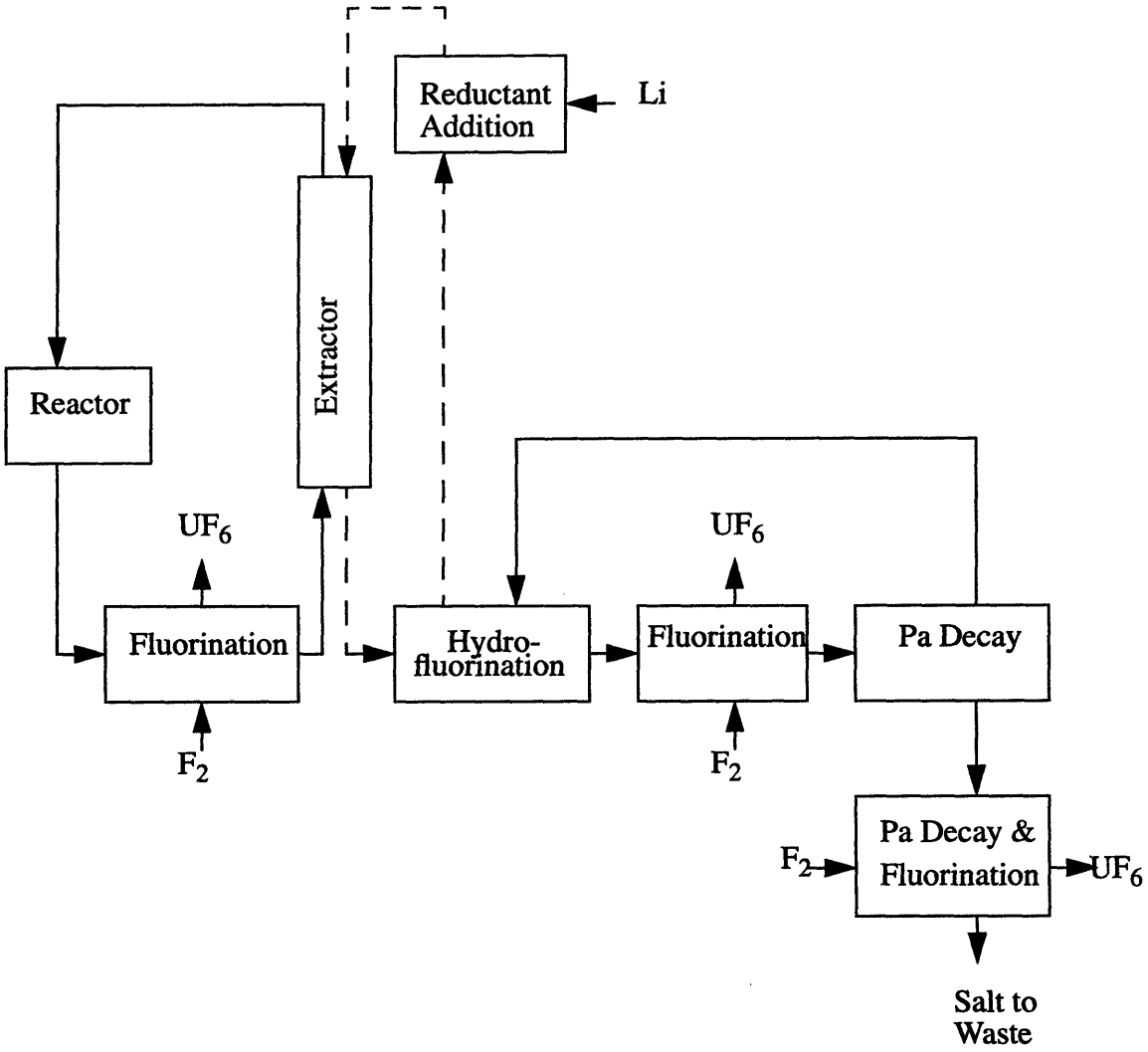

Figure 3.2: Flowsheet for Isolation of Uranium and Protactinium by Fluorination-Reductive Extraction [30]

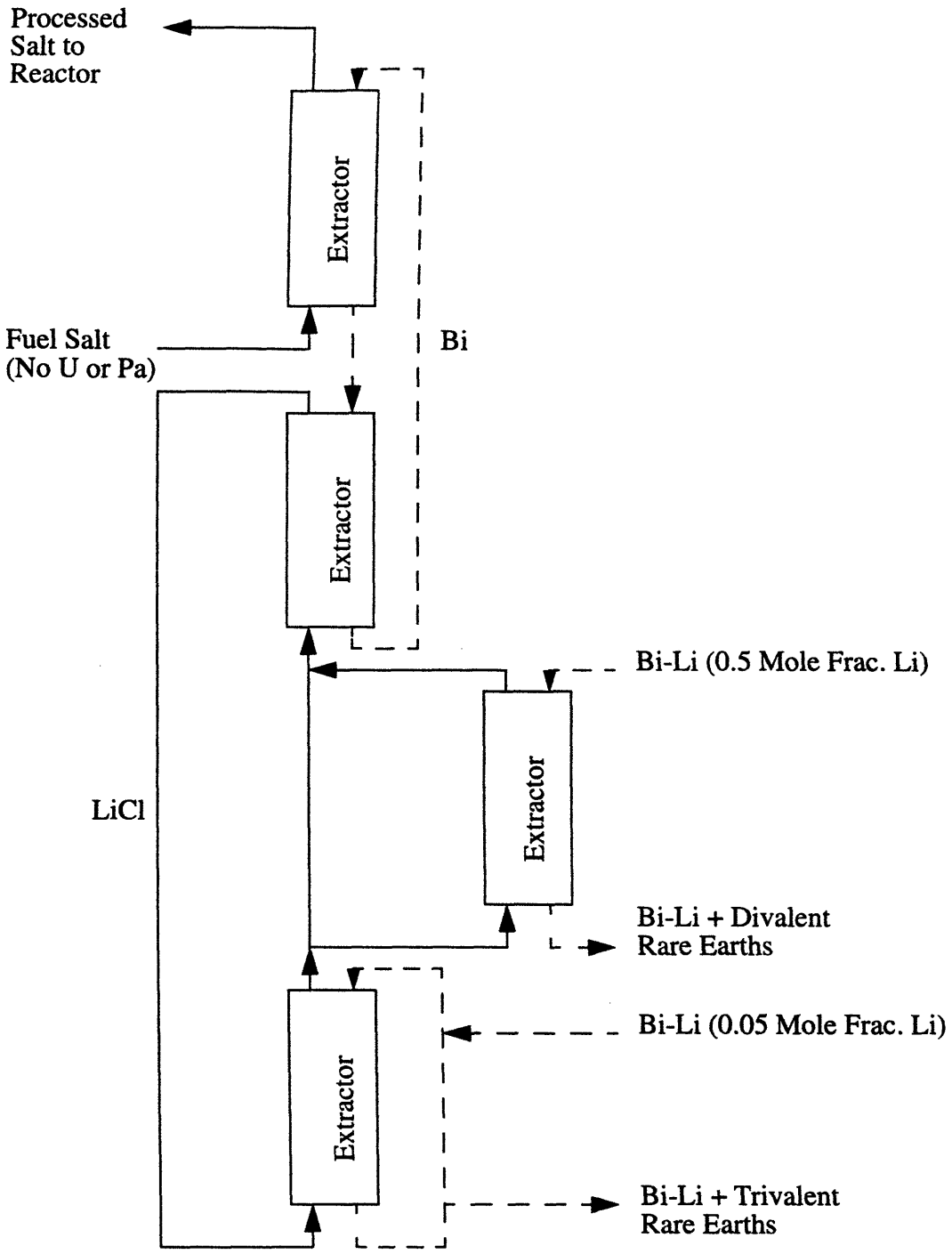

Figure 3.3: Metal Transfer Process for Removal of Rare Earths Illustrated with Two Stages, Any Number of Stages Possible In Order to Increase System Efficiency [30]

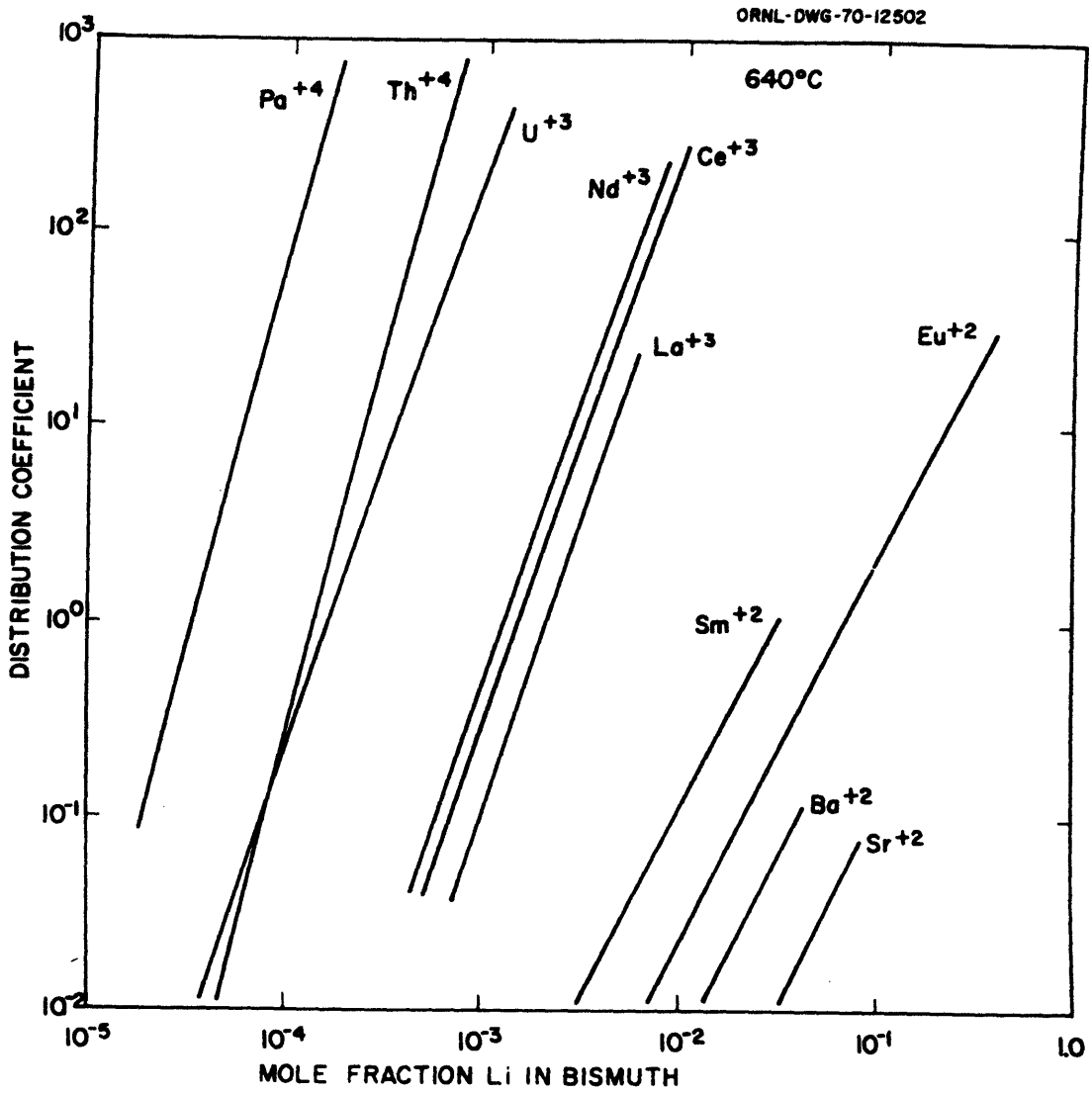

Figure 3.4: Distribution Coefficient Data Between Lithium Chloride and Bismuth [30]

The processing system as designed for the ORNL molten salt breeder reactor had a total cycle time of 10 days and an efficiency of 40%. This cycle time was the total time required for the entire volume of fuel salt to be processed. The efficiency of the processing system is a measure of the fission product removal capability. If all fission products are removed from the salt in a single pass through the chemical processing system, the efficiency approaches 100%. Because the ORNL Molten Salt Breeder Reactor (MSBR) had a proposed efficiency of 40%, the total cycle time must be replaced with an effective processing time. For this particular system, the effective processing time is 25 days. These limits were set primarily by economics [30].

3.8 Required Improvements

The latest design of large-scale molten salt breeder reactors requires improvement in two primary areas before the characteristics necessary for a serious global warming mitigation effort may be satisfied. The first is the chemical processing system, where the removal of fission products should be done continuously to achieve the maximum benefit. The equipment must therefore be capable of continuous, sequential operation. The second area is the cooling systems. The potential hazards associated with the sodium fluoroborate and steam systems should be eliminated. During the development stages of the MSRE in the 1970s, the use of passively safe systems was not emphasized. The incorporation of these systems would result in a more acceptable, inherently safe reactor system. With these proposed augmentations to the base design, the molten salt breeder reactor would provide an attractive alternative for an environmentally sustainable, global-scale power system.

Chapter 4

Chemical Processing

4.1 General

The processing of molten salt fuels has been eliminated from the most recent designs based upon the adverse economics, performance, reliability, safety, and political forces associated with these complex systems. The development of continuous fluorinators was never accomplished for this primary reason. Due to the cancellation of research on the chemical processing of molten salt fuels, the processes were never run sequentially and reconstitution efforts were halted, providing no proof of the concept.

To ensure the removal of fission products from the fuel salt, a reliable system must be employed. This would require either extensive evaluation and development of the continuous fluorinators and reconstitution procedures essential to the proposed process or development of a totally new design of the chemical processing plant. One new approach is presented here.

4.2 One Step Processing

Initial concern in past development efforts was that the protactinium be separated from the fuel salt to isolate it from the neutron flux. The protactinium could then be stored, allowing the decay to ^{233}U. This same end result may be realized regardless of whether the protactinium has been isolated from the carrier salt if it can be protected from the neutron flux. Therefore, the fluorination-reductive extraction technique for the removal of the uranium and protactinium will be unnecessary if the fuel salt in its entirety is stored to allow for the protactinium decay. In addition, there would be no need for fuel salt reconstitution. Applied to the ORNL MSBR, 9 kg/MWe of fissile material would be required if the pro-

tactinium were to be protected from the neutron flux for two half lives. This is slightly higher than the 5 kg/MWe of fissile material employed in the liquid metal fast breeder reactor.

This directs the line of inquiry to methods for removal of the rare earths from a fuel salt which contains the uranium and protactinium. Figure 3.4 shows that the distribution coefficients for uranium and protactinium follow the same behavior as that exhibited by the thorium in the metal transfer process. By contacting the unprocessed fuel salt countercurrently with a bismuth stream which is then countercurrently contacted with a lithium chloride stream, the rare earth separation from the fuel salt may be achieved without the prior removal of the uranium and protactinium. Doing this simplifies the processing plant to the system illustrated in Figure 3.3. By eliminating the fluorination-reductive extraction removal of the uranium and protactinium, much of the previously required equipment becomes unnecessary. With only one step, this entire process has been successfully proven in laboratory trials.

The metal transfer process may be run in a semi-continuous manner. This means that the extraction would be performed continuously until the equipment is taken off-line for replenishment of the reductants. With no net consumption of the bismuth or lithium chloride, the time between replenishments can be maximized. Using several systems in parallel, the load which would be routed to one system during normal operation could be rerouted through the on-line system when the first is taken off-line. This would provide uninterrupted, continuous processing.

4.3 Process Efficiency and Cycle Time

The processing system designed for the molten salt breeder reactor at ORNL was designed to have had an efficiency of 40% and a total cycle time of 10 days. These conservative

limits were based on economic factors. According to J. R. Engel, an ORNL engineer on the molten salt project, it was thought desirable at the time for the volume of reductants consumed and the amount of equipment required to be minimized. The resultant design increased the breeding capacity of the system, but did not maximize the potential of the processing system [32].

The modified processing system considered here is not hindered by economic limitations. The quantity of reductants and amount of equipment utilized are purely economic considerations. Increasing the number of stages in the processing system and the total system throughput, the efficiency and cycle times may be adjusted to any desired values. It has been postulated that the processing time may be shortened to 1 day with an approximate efficiency of 100% as a way to enhance the safety of molten salt reactors [33].

4.4 The Fuel Decay Heat

The resultant decay heat arises from the decay of fission products which are not removed from the fuel salt at the time of an accident. The fission products which have been removed from the reactor during processing are not available to participate in a reactor accident. This is especially true if the wastes are removed from the reactor site. Therefore, the only fission products which contribute to the decay heat load are those which remain in the primary system.

The quantity of fission products remaining in the salt must be determined in order to calculate their decay heat contribution. This may be done by considering the steady state operation of the plant. Considering only simple decay as an approximation, the rate of change of the number of atoms, N, without processing may be expressed as:

$$\frac{dN}{dt} = F - \lambda N, \tag{4.1}$$

where F is the production rate of the isotope and λ is the decay constant. With an on-line processing system with an efficiency, ζ, of 100% and a total processing cycle time of π, this equation may be modified to the following relationship:

$$\frac{dN}{dt} = F - \lambda N - \frac{N\zeta}{\pi}. \tag{4.2}$$

Defining an effective processing time, Π, equal to π/ζ, this may be rewritten as the relationship:

$$\frac{dN}{dt} = F - \lambda N - \frac{N}{\Pi}. \tag{4.3}$$

Here, the rate of removal due to processing is simply the inverse of the effective processing cycle time, Π. Assuming that no fission products are present at the time of start-up, the inventory of a particular fission product species at time t is obtained in the form [20]:

$$N(t) = F\frac{\left(1 - e^{-\left(\lambda + \frac{1}{\Pi}\right)t}\right)}{\lambda + \frac{1}{\Pi}}. \tag{4.4}$$

Thus, the steady state inventory of each isotope is equal to $F/(\lambda + 1/\Pi)$. For short-lived isotopes, the value of λ is much greater than the reciprocal of the processing cycle time. Therefore, at equilibrium their inventory will reach a value of F/λ. This is equal to the value attained with no processing of the fuel. For long-lived isotopes ($\Pi<1/\lambda$), the reciprocal of the processing cycle time is the dominant term. This results in an approximately linear build-up of these fission products to a value of Ft where t is the elapsed operating time. The largest possible value of this inventory is $F\Pi$. The maximum inventory of long-lived fission products in a system which has no on-line chemical processing is given by FT, where T is the operational time interval. Therefore, the ratio of the fission product inventory for a system with chemical processing to the inventory in a comparable solid fuel

reactor is $F\Pi/FT$. From this relation it may be seen that the chemical processing system is capable of reducing the fission product inventory by a factor of Π/T in comparison to a comparable solid fuel reactor [20]. This steady state approach accurately predicts the fission product inventory due to the equilibrium steady state operation of a molten salt breeder reactor with on-line chemical processing.

With the relative fission product concentrations known, the decay power produced with processing must be computed. For systems without on-line fission product removal, an empirical correlation is used to estimate the decay power produced as a function of the steady state power at which the reactor had operated (P_0), the length of time in seconds for which it had operated (t_0), and the length of time elapsed after reactor shutdown (t). For a thermal system fueled by ^{235}U, the decay power, $P(t)$, is given by the following relation [5]:

$$P(t) = 6.6\times10^{-2}P_0\left(t^{-0.2} - (t+t_0)^{-0.2}\right). \tag{4.5}$$

The molten salt reactor consumes a uranium-233 fuel. An inspection of the fission product spectrum for ^{233}U and ^{235}U reveals that there is little difference in the fission product distributions [34]. Therefore, the decay heat produced with a ^{233}U fuel may be roughly approximated by the relation for ^{235}U.

The molten salt reactor processing system complicates the decay heat calculation as it preferentially removes long-lived fission products. For this reason, the contribution of each fission product species to the overall decay heat must be estimated. For a particular fission product species, the power generated by the decay is simply the activity of that species times the amount of energy, C, which is imparted to the fuel salt with each decay. For beta and gamma decay of fission products, C is approximately 8 MeV [35]. Summing over

all fission products yields the total decay heat. This may be expressed mathematically with the following relation:

$$P(t) = C\int_0^\infty \lambda N(\lambda)\, e^{-\lambda t} d\lambda. \tag{4.6}$$

It may be recognized that $P(t)$ is the Laplace transform of the quantity, $C\lambda N(\lambda)$. Solving for $N(\lambda)$ gives the result:

$$N(\lambda) = \frac{1}{C\Gamma(0.2)} 6.6\times10^{-2} P_0 \lambda^{-1.8} (1 - e^{-\lambda t_0}), \tag{4.7}$$

where $\Gamma(a)$ is the gamma function. The gamma function is defined by the relationship:

$$\Gamma(a) = \int_0^\infty x^{a-1} e^{-x}\, dx. \tag{4.8}$$

In order to determine the decay power produced in association with chemical processing, the effect of fission product removal must be taken into consideration. For short-lived fission products ($\lambda > 1/\Pi$), the concentration equals that of the system without processing, $N(\lambda)$. For long-lived fission products, the concentration is reduced by a factor of Π/T, becoming equal to $\Pi N(\lambda)/T$. The decay power produced may then be approximated by, once again, summing their respective decay rates over all fission products. This summation may be written:

$$P_{proc}(t) = C\left(\frac{\Pi}{T}\int_0^{\frac{1}{\Pi}} \lambda N(\lambda)\, e^{-\lambda t} d\lambda + \int_{\frac{1}{\Pi}}^\infty \lambda N(\lambda)\, e^{-\lambda t} d\lambda \right). \tag{4.9}$$

The following relationship results:

$$P_{proc}(t) = P(t) + \frac{6.6\times10^{-2} P_0}{\Gamma(0.2)} \left(t^{-0.2}\left(\frac{\Pi}{T} - 1\right)\gamma\left(0.2, \frac{t}{\Pi}\right) - (t + t_0)^{-0.2}\left(\frac{\Pi}{T} - 1\right)\gamma\left(0.2, \frac{t + t_0}{\Pi}\right)\right), \tag{4.10}$$

where $\gamma(a, b)$ is the incomplete gamma function. This function may be represented by the infinite series:

$$\gamma(a,b) = \sum_{n=0}^{\infty} \frac{(-1)^n b^{a+n}}{n!\,(a+n)}. \tag{4.11}$$

For large values of b, this summation converges to large values, yielding impossibly large, unphysical results. For application to decay heat with processing, this behavior may be experienced at high values of $(t+t_0)$ or at low values of Π.

A comparison of the decay power with and without on-line fission product removal is illustrated in Figure 4.1 for an operating time of 1 year at 2250 MWth. The effect of the fission product removal is greatly to reduce the decay power burden of the system in the long term, however the short term decay power produced remains virtually unaltered.

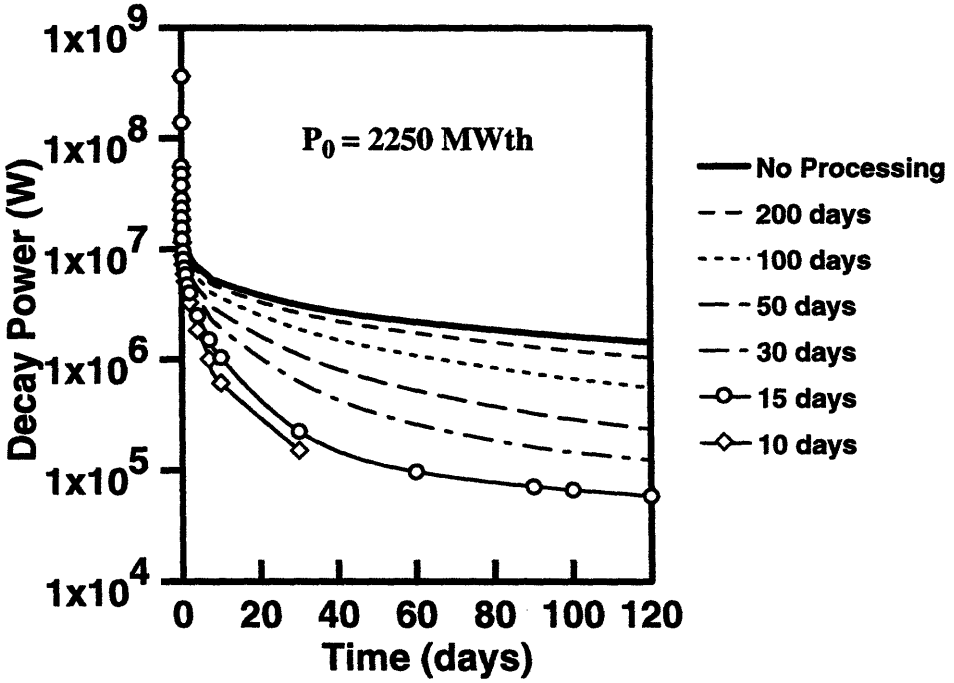

Figure 4.1: Comparison of Fission Product Decay Power With and Without Chemical Processing, Curves Shown for Different Processing Times

With this system, the decay heat removal system must be capable of removing decay heat loads of the magnitude experienced in solid fuel reactors for a length of time approximately equal to that of the processing time. Thereafter, the decay heat generated is diminished to a factor Π/T times the decay heat of a system without processing.

Chapter 5

Heat Transfer Performance

5.1 General

Improvement of the cooling systems of the molten salt breeder reactor would increase the safety inherent in the plant. With modifications, the risks associated with accident conditions may be reduced. Application of technologies which have undergone substantial developmental effort since the original design of the molten salt reactor may augment the overall plant safety. The latest design of a large-scale molten salt breeder reactor was the Molten Salt Breeder Reactor (MSBR) developed at the Oak Ridge National Laboratory [36]. A schematic of this reference design is included in Appendix A along with pertinent primary system and primary heat exchanger data [29].

Safety is vital during routine operations as well as during accident conditions. During regular operation, the choice of compatible cooling materials eliminates the problems associated with potential fuel leaks. The use of sodium fluoroborate and steam, as discussed in Section 3.6, introduces concerns such as the potential mixture of water with the salts, the pressurization of the primary system, and the need for duplex tubes in the steam generator. This may be avoided with the use of a LiF-BeF_2 secondary coolant, a helium tertiary coolant, and gas turbines. During accident conditions, the use of passive safety systems insures that the fission products do not become volatilized with high temperatures and that all components do not overheat. Two accident scenarios which may be countered by the application of passive safety features are pump failure and drainage of the fuel salt from the primary loop. Utilizing natural circulation, the fuel salt will continue to circulate in the absence of a pump. Routing the drained fuel salt to an alternate location, natural convection may be employed to remove the decay heat of the reduced fission product con-

centration. The inclusion of these features in the molten salt breeder reactor design can produce a safer system capable of meeting the needs for a serious global warming mitigation effort.

5.2 LiF-BeF_2, Helium, and Gas Turbines

The original molten salt reactor experiment at ORNL used a LiF-BeF_2 coolant which rejected its heat to an air-cooled radiator at a minimum temperature of 566°C. Due to the large knowledge base available for steam turbine systems, steam was chosen as the tertiary coolant for the MSBR, leading to the replacement of the LiF-BeF_2 with NaF-$NaBF_4$ due to the respective melting temperatures of these materials. This new choice of coolant presented technological challenges, but these challenges were not considered insurmountable [24]. Given the advancements in gas turbine technology, it is no longer necessary to accept the difficulties presented with steam turbines.

The adversity related to the potential mixture of the secondary coolant salt with the fuel salt or tertiary coolant is minimized with the use of LiF-BeF_2. Providing the base for the fuel salt, LiF-BeF_2 is already present in the primary circuit. A leak would simply increase the quantity of base salt present with no detrimental reaction. The tertiary coolant, helium, has previously been bubbled through the fuel salt to facilitate the removal of gaseous fission products, demonstrating the compatibility of this inert gas with the LiF-BeF_2 base salt. Therefore, the use of these fluids would eliminate the hazardous interactions of the fluids utilized in the molten salt breeder reactor.

With the use of the sodium fluoroborate-steam system, the feedwater temperature of the steam had to be carefully monitored to evade the freezing of the sodium fluoroborate in the steam generator tubes. Utilizing a helium gas turbine system, the system may be operated at higher temperatures. The secondary coolant will span a temperature range of

approximately 566°C to 704°C. These elevated temperatures are suitable for gas turbine application with a system efficiency of approximately 34%. Raising the temperature will result in higher efficiencies [37]. One means of doing this is to eliminate the secondary coolant loop. With no interactions between the fuel salt and helium gas, doing this would not sacrifice the safety of the system. By eliminating the preheaters and utilizing the more efficient gas turbines, the safety of the plant is enhanced.

5.3 Natural Circulation of the Fuel Upon Pump Failure

The planning of a nuclear power plant must anticipate potential equipment failures. One such failure that may occur in a molten salt reactor is that of the pumps in the primary loop. Loss of circulation of the fuel salt could lead to the overheating of the fuel. If a fuel temperature of over approximately 1000°C were to be reached, the fission products in the fuel could volatilize.

In order to prevent the loss of fuel salt flow, the reactor system may be designed to accommodate natural circulation and cooling in the primary coolant circuit. The reference MSBR design, shown in Figure A.1, does not create any buoyancy head in the fuel. This may be done by elevating the primary heat exchanger. An example configuration is illustrated in Figure 5.1. In addition to the elevation of the heat exchanger, the geometry of the piping may be varied to allow for increased heating by delayed neutrons in portions of the loop and increased cooling by radiation and natural convection in others.

At the onset of pump failure, an initial transient will ensue. The change in the mass flow rate with time may be determined from the conservation of momentum as applied to the primary loop. This is the following [38]:

$$\sum_k \left(\frac{L_k}{A_k}\right)\frac{\partial}{\partial t}\dot{m} = \Delta p_{pump} - \Delta p_{friction} - \Delta p_{form} - \Delta p_{acceleration} + \Delta p_{buoyancy}. \qquad (5.1)$$

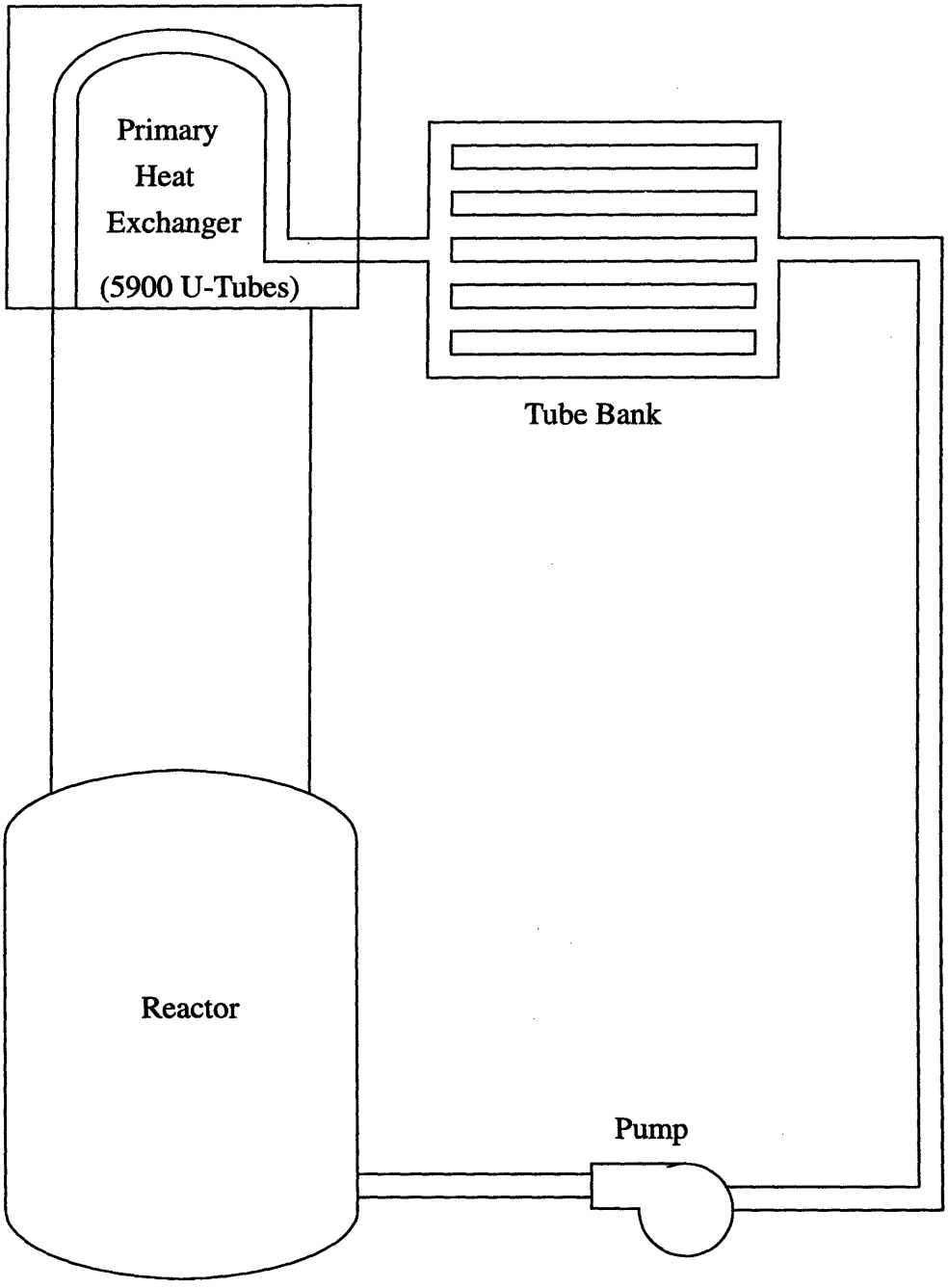

Figure 5.1: A Schematic Diagram of an Example Natural Circulation Configuration with Elevation of the Heat Removal Systems to Drive a Naturally Circulating Flow and a Tube Bank which Allows for Heat Rejection in the Event of Primary Heat Exchanger Failure

For the case of pump failure, the Δp_{pump} term may be discarded. To maintain adequate primary flow, it is desired that the mass flow rate not fall too dramatically. Therefore, efforts must be made to minimize $\Delta p_{friction}$, Δp_{form}, and $\Delta p_{acceleration}$ while maximizing $\Delta p_{buoyancy}$. The $\Delta p_{friction}$ term includes the losses through the components in the primary loop: the core, primary heat exchanger, and pump.

5.3.1 The Core

By changing the core configuration with an increase in the diameter of the graphite flow channels, the pressure drop through the core region may be decreased. This must be carefully balanced, however, with the increased damage to the moderating graphite incurred due to the rise in internal graphite temperature. An alternate method would be to decrease the height of the reactor while simultaneously increasing the core diameter and number of channels.

5.3.2 The Primary Heat Exchanger

The primary heat exchanger presents additional pressure losses, however a change in the dimensions which would decrease the pressure loss would also sacrifice valuable heat transfer area and is therefore undesirable. For the case of pump failure, it may be assumed that the pumps in the secondary loop fail as well, rendering the primary heat exchanger ineffective for heat removal. Therefore, an alternate means for heat rejection must be provided. One method for providing this additional means for heat rejection is a tube bank. Allowing both natural convection cooling of the tubes in the bank and thermal radiative losses to the surroundings, the heat may be effectively rejected.

5.3.3 The Pump

Finally, the pump may be bypassed using an arrangement such as that shown in Figure 5.2. In this configuration, flow will only proceed through the bypass route if the pressure

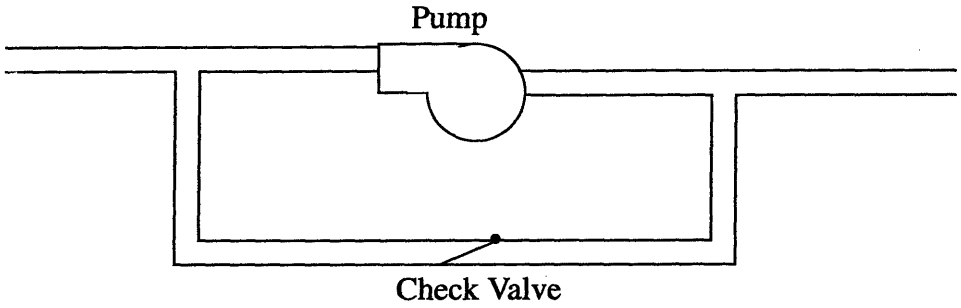

Figure 5.2: Bypassing of the Failed Pump

at the pump inlet is greater than that at the outlet, providing the force to open the check valve. Upon opening, the bypass route will be the preferred path due to lower pressure losses. Therefore, this mode of operation is passive.

Buoyancy constitutes the sole driving force for the mass flow rate in the absence of the pump. In order to maximize this term, the hot flow of fluid from the core must be routed to an elevated heat exchanger. By rejecting the heat at a higher point than where it is produced, the varying densities of the fuel create a buoyancy head which will induce flow. Employing a greater height will yield a greater buoyancy head, driving a greater mass flow rate. Combining this approach with the means to reduce the friction and form pressure losses, adequate natural circulation of the fuel salt may be achieved.

In order to determine the geometry required for the potential use of this flow regime, the induced mass flow rate must be determined. Replacing the pressure change terms with more detailed expressions, a solution may be found for the mass flow rate as a function of time after the pump failure. This is done in Appendix B. This mass flow rate approaches an equilibrium flow rate. The results of the calculation are summarized in Table 5.1. It may be seen that a height of 15 m is needed in order to achieve an adequate mass flow rate. These results were obtained with a core one quarter the height of the referenceMSBR

Table 5.1: Natural Circulation System Parameters Required to Avoid Fission Product Volatilization

Height	15 m
Riser Diameter	4 m
Number of Tubes in Bank	328
Bank Tube Diameter	0.25 m
Tube Bank Length	22 m
Piping Diameter	1 m
Initial Mass Flow Rate	2906 kg/s
Equilibrium Mass Flow Rate	850.91 kg/s
Time to Equilibrium	15 s
Maximum Fuel Temperature	840°C
Fuel Temperature Limit	1000°C

design possessing four times the number of flow channels. The four loops utilized in the reference design were carried over to this analysis.

The rapid deceleration of the system is caused by the high value of the friction pressure loss of 0.89 MPa caused by the primary heat exchanger. The time for the flow to cone to equilibrium may be compared to the flow decay time constant in order to insure that this quick flow slowdown is reasonably correct. In the event of pump failure without subsequent pump coastdown, the time constant for turbulent flow is given by [38]:

$$\tau = \frac{\dot{m}_0^{1.2}}{0.8\Delta p_{loss}} \sum_k \frac{L_k}{A_k}. \tag{5.2}$$

For the geometry under consideration, this yields a value of 4.63 s. Therefore, the 15 s estimated for the flow to come to a naturally convective equilibrium is in reasonable agreement. This time scale may be increased slightly by considering the effects of the pump inertia coastdown (e.g., due to use of a flywheel on the pump rotor.).

Additional methods may be utilized to augment the buoyancy head. This may be done by bubbling helium gas into the heated fuel salt stream, further reducing the density. This bubbling may be accomplished with the use of a tank of the helium gas and an appropriately set regulator valve which would limit the rate of release of helium into the fuel salt. A system which could do this is illustrated in Figure 5.3.

5.4 Natural Convection Cooling of Drained Fuel Salt

In the event of an unexpected condition from which the reactor cannot be expected to recover, the fuel salt may be drained from the primary system. This action will stop the fission chain reaction due to the elimination of neutron moderation. The fuel may then be routed to specially designed tanks where it may be cooled passively.

The removal of all fission products from the fuel salt is an unrealistic goal, and therefore the decay power must be rejected. Section 4.4 details the calculation of the amount of decay power which will be present with the modified processing system. In order to ensure that the passive operation of the decay heat removal system, a natural convection system may be employed.

5.4.1 Geometry

Natural convection of air across the surface of the fuel salt is enabled by the geometry of the cooling tanks. An example of such a geometry is displayed in Figure 5.4. The height of the chimney produces a buoyancy head which drives the flow of air across the fuel salt. The air used would be drawn from and returned to the atmosphere. By varying the height of the channel of air above the fuel, the air velocity may be altered to achieve the optimal balance between convective heat transfer and the friction experienced by the flow through the channel. The depth of fuel in the tank may also be varied to spread the decay heat load over an increased surface area. By covering the fuel salt tank with a material transparent to

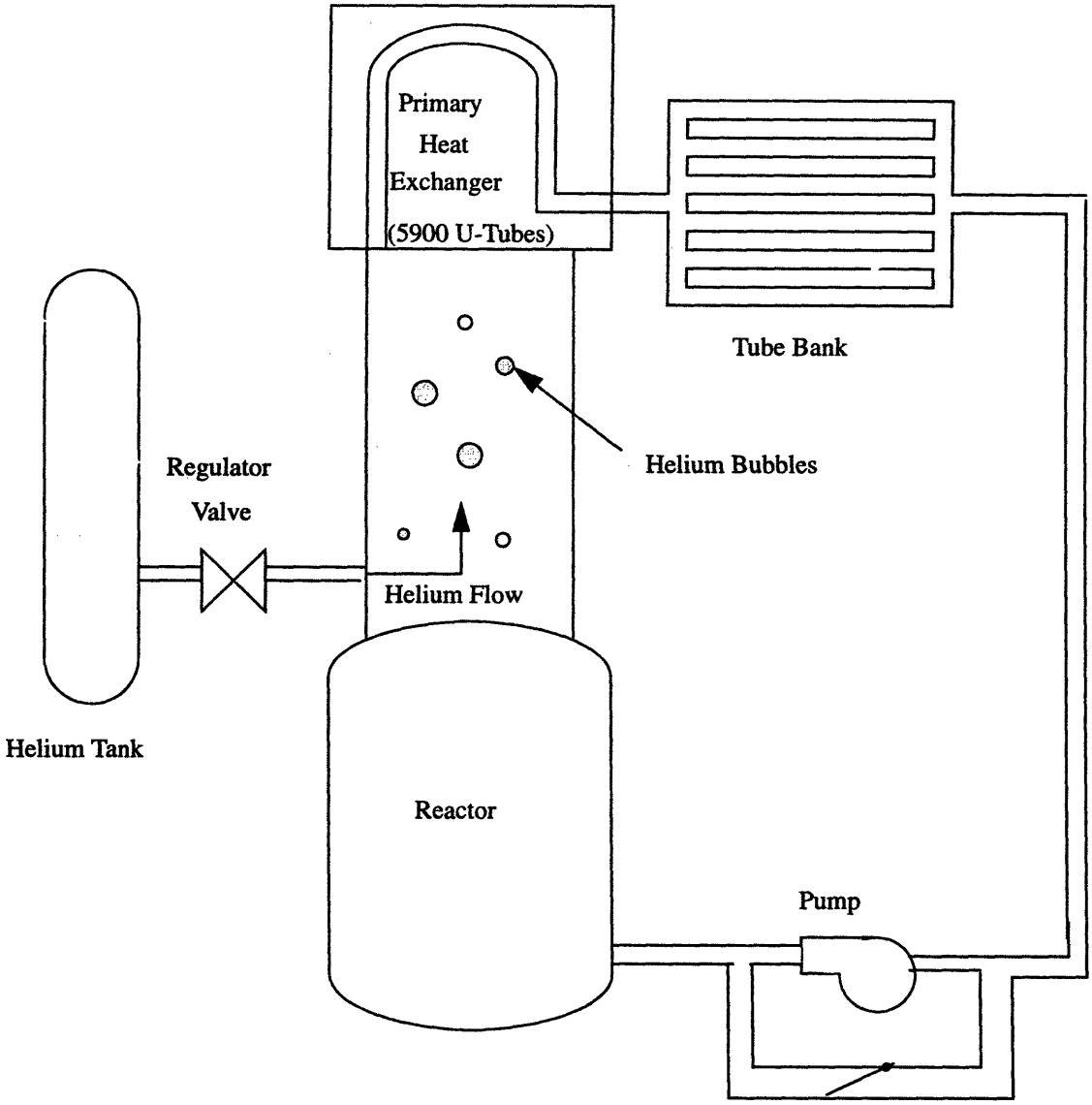

Figure 5.3: Schematic Diagram of a System for Reducing Density of Fuel Salt in the Power Plant Hot Leg by the Insertion of Helium Gas In Order to Drive a Naturally Circulating Flow for Reactor Cooling

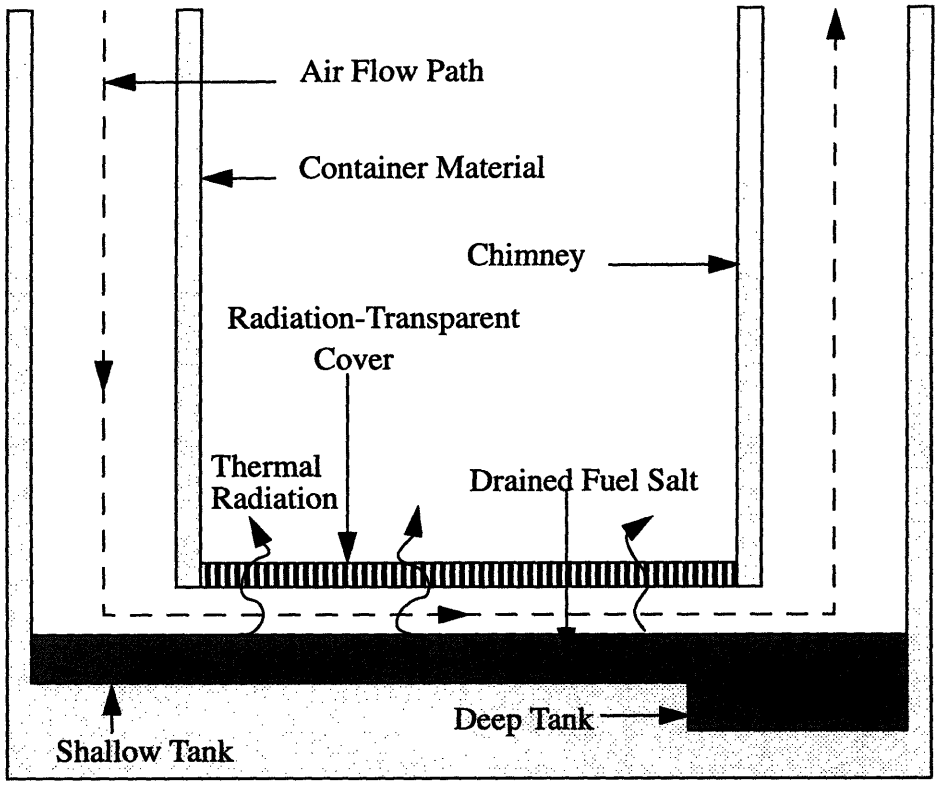

Figure 5.4: Side Section View of an Example Geometry of a System for Air Cooling of the Drained Fuel Salt by Natural Convection

the emitted thermal radiation, additional heat may be rejected by means of radiation heat transfer. The structure may also be cooled in order to insure that it does not overheat. This may be done by immersing the system in a coolant bath or by natural convection cooling.

In order for this system to induce the air flow path indicated in Figure 5.4 effectively, the tank must be designed to heat one side of the salt preferentially. This may be done by increasing the fuel salt depth at the end of the horizontal air flow path. An alternate method is the elimination of fuel salt in the entrance region, however this method sacrifices heat transfer area. For this reason the first method should be used.

5.4.2 Calculation of the Fuel Temperature

Upon the selection of the geometry, the heat removal capacity of the system may be deter-

mined. The mass flow rate of air depends upon the temperature of the fuel salt. This mass flow rate then dictates the rate of removal of heat from the fuel salt.

A detailed description of the model used to calculate the fuel temperatures is given in Appendix C. Using heat and mass balances to calculate the air and salt temperature fields, coupled with a balance of the momentum loss and buoyant forces, the mass flow rate induced by the geometry may be determined. This mass flow rate of air is then used as input to an implicit finite difference calculation of the temperature profile obtained through the salt as a result of conduction. Possessing a low expansivity, the buoyant mixing of the fuel salt due to the temperature gradients within the salt will not occur. This method is used over a series of time intervals, determining the salt temperature profiles as a function of time.

5.4.3 Results

Repeating the calculation with varying geometries, an optimal design for the cooling tanks may be achieved. For a molten salt breeder reactor of the ORNL reference design which has operated at 2250 MW for a period of one year with a processing cycle time of ten days, Table 5.2 summarizes the resulting parameters. The maximum salt temperature is experienced at the base of the deep fuel tank 42 minutes after the draining of the fuel. The temperature profile through the salt at this time is shown in Figure 5.5. It is evident from these results that the proposed system provides an effective, passively safe means for decay heat removal.

5.4.4 Enhancement of Cooling Capacity Using Heat Storage

The cooling capacity required for the system developed here is determined by the heat produced within the first 24 hours after reactor shutdown. With continual reduction of the decay heat magnitude, the tank proves to be oversized for the majority of the time over which it is needed. In order to augment the system's heat removal capabilities until the

Table 5.2: Parameters of an Example Air Natural Convection Cooling System as Applied to the Molten Salt Breeder Reactor Reference Design

Chimney Height	60 m
Width of Duct Above Fuel Salt Tank	0.02 m
Width of Tank	70 m
Length of Shallow Tank	5 m
Length of Deep Tank	11.4 m
Depth of Shallow Tank	0.025 m
Depth of Deep Tank	0.05 m
Maximum Temperature	856.48 °C
Maximum Allowable Tamperature	1000 °C
Time to Maximum Salt Temperature (at bottom of tank)	42 min

decay heat falls to reduced levels, a means of storing heat during times of high fuel power may be used. In an example system, a layer of solid salt may be used in the tanks as a temporary heat sink. This system is illustrated in Figure 5.6. As the drained fissile fuel salt comes into contact with the non-fissile solid salt, the solid salt heats and then begins to melt. The process of melting requires that an amount of energy equal to the product of the solid mass and the heat of fusion of the salt be consumed, further cooling the drained fuel salt. The length of time over which the heating and melting occurs is determined solely by the depth of the salt. After the salt has thoroughly melted, the internal energy of the fuel salt will be distributed over a greater salt mass, thereby lowering the overall temperature.

The use of solid salt in the cooling tanks was applied to the MSBR reference design. Providing a depth of solid salt in each tank equal to that of drained fuel salt, with the solid salt initially being at room temperature, greatly reduced the cooling tank parameters. Appendix D describes the modeling of this the natural convection cooling system with initially solid salt. Figures 5.7 through 5.10 illustrate the temperature profiles across the salt

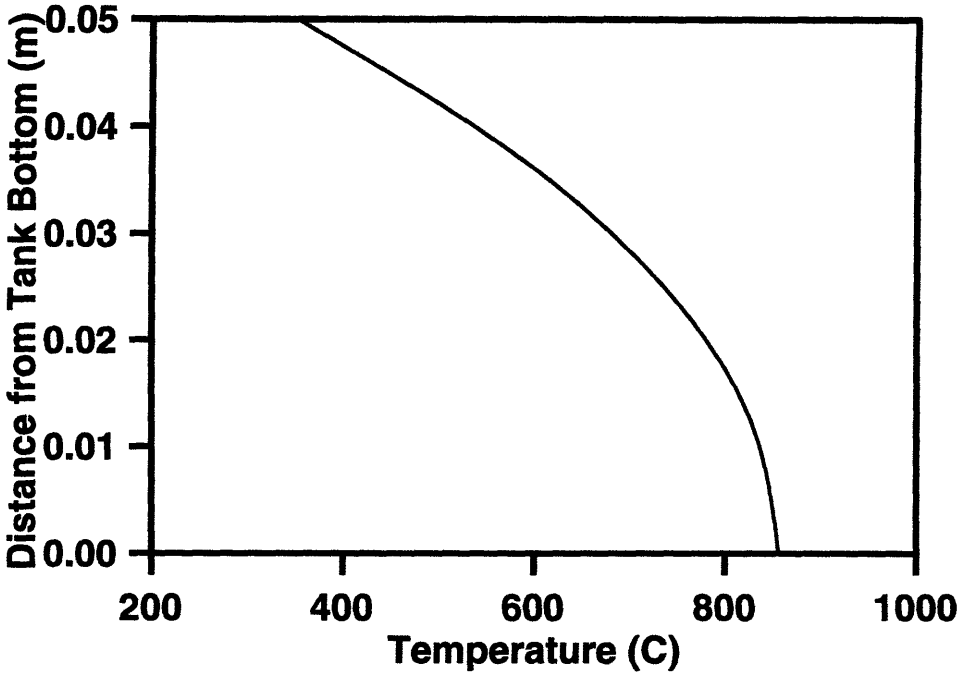

Figure 5.5: Temperature Profile Through the Fuel Salt

and the temperature at various locations through the salt as a function of time. Although the initially solid salt does not melt in the shallow tank, it decreases the maximum temperature in the fuel salt by providing a means for heat storage. In the deep tank, this initially solid salt layer does melt. This is clearly shown in Figure 5.10 for the node located 0.05625 m from the bottom of the deep tank for example. This node remains at the melting temperature for the period of time over which the node melts. Table 5.3 lists the results for the system parameters required with the use of initially solid salt. With a reduction in the chimney height to 30 m and the use of initially solid salt, the maximum temperature reached is reduced to 722.24°C.

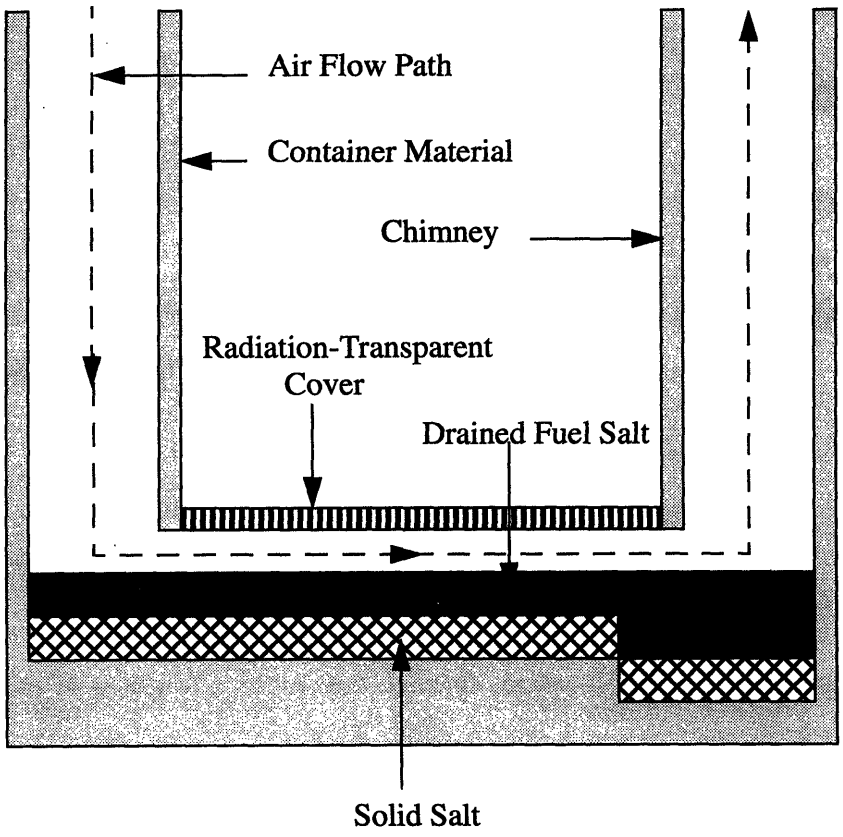

Figure 5.6: Side Section View of the Use of Initially Solid Salt in the Natural Convection Cooling System

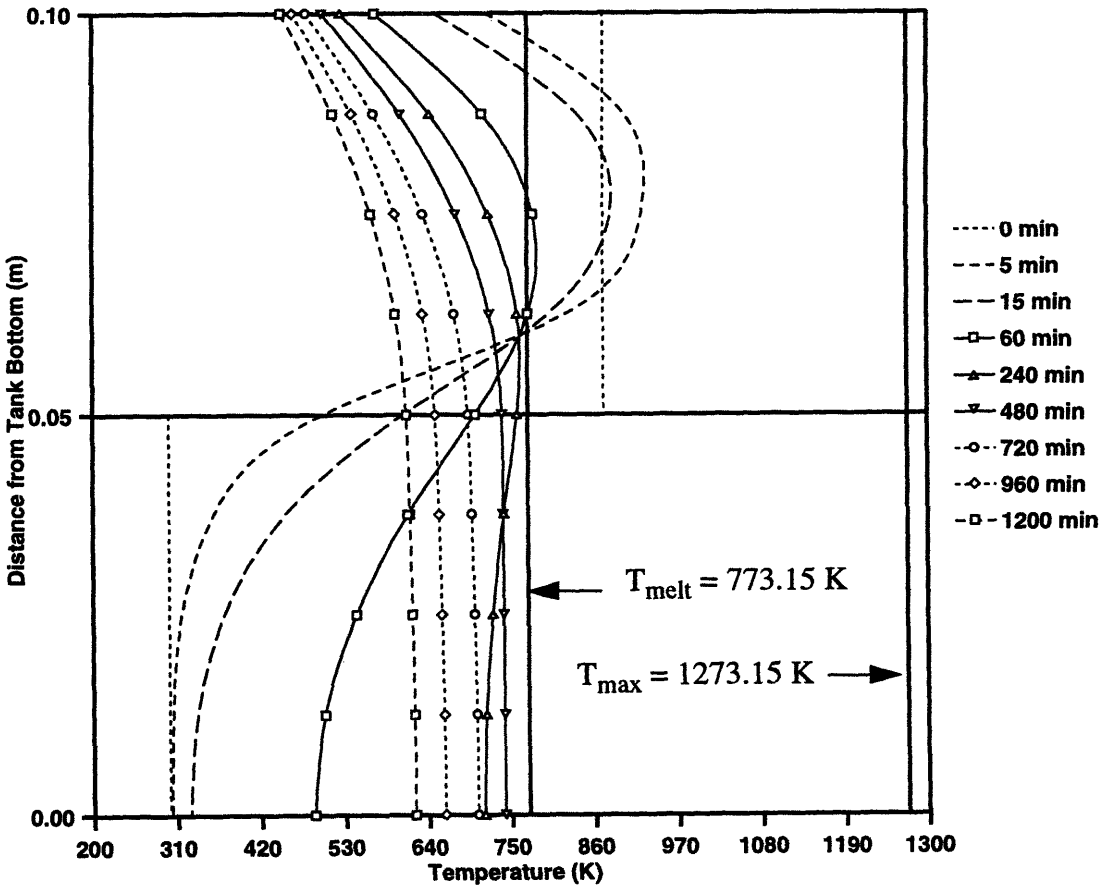

Figure 5.7: Temperature Profile through the Depth of the Fuel Salt and Non-fissile Salt in the Shallow Tank as a Function of Time

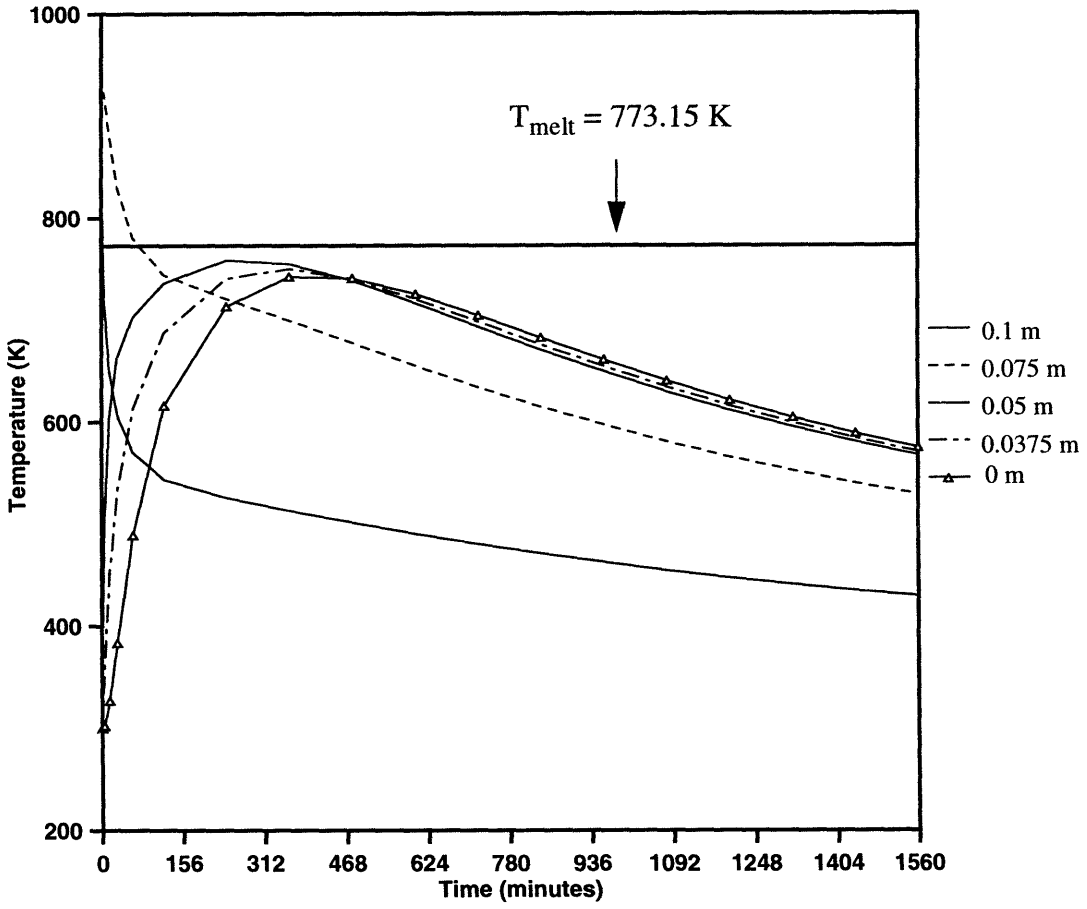

Figure 5.8: Salt Temperature at Various Distances from the Bottom of the Shallow Tank as a Function of Time

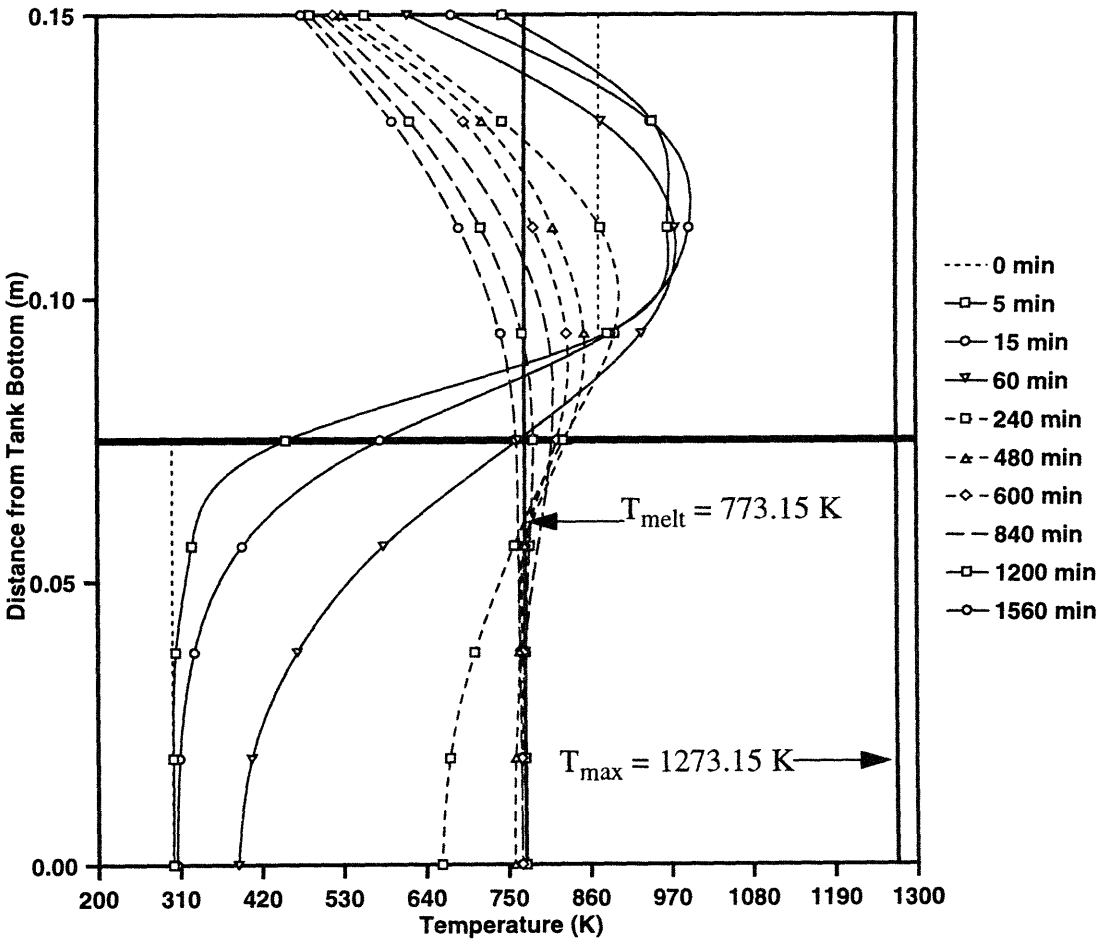

Figure 5.9: Temperature Profile through the Depth of the Fuel Salt and Non-fissile Salt in the Deep Tank as a Function of Time

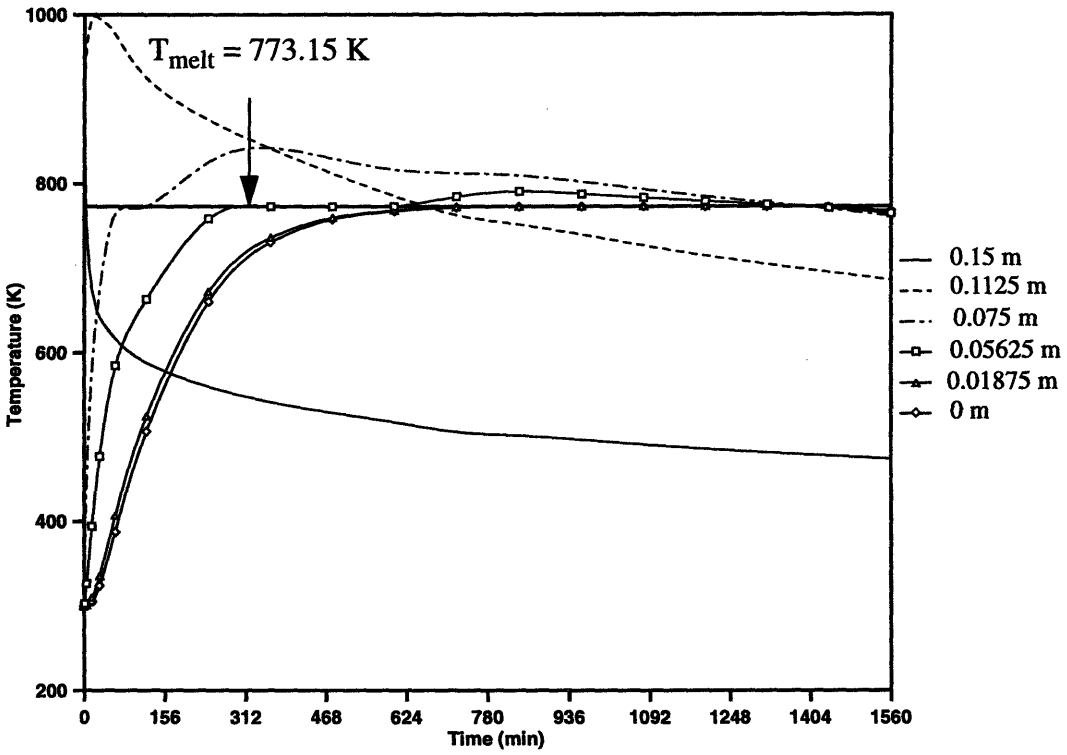

Figure 5.10: Salt Temperature at Various Distances from the Bottom of the Deep Tank as a Function of Time

Table 5.3: Parameters of the Air-Natural Convection Cooling System Using an Initially Solid Salt Heat Sink as Applied to the Molten Salt Breeder Reactor Reference Design

Chimney Height	30 m
Width of the Duct Above Fuel Salt Tank	0.02 m
Width of Tank	60 m
Length of Shallow Tank	2 m
Length of Deep Tank	9.49 m
Depth of Shallow Tank	0.05 m
Depth of Deep Tank	0.075 m
Maximum Temperature	722.24 °C
Maximum Allowable Temperature	1000 °C
Time to Maximum Temperature	15 min
Ratio of Depth of Fuel Salt to Solid Salt	1

5.4.5 Toxic Effluents

The employment of natural convection cooling system using air for fuel cooling has several public health implications. These are the potential production of hydrofluoric acid and beryllia which may be carried in the air flow. The air used would be drawn from and returned to the atmosphere. Use of appropriate filters may control the quantities released into the atmosphere, however the large pressure drop associated with the filters would eliminate the possibility of establishing natural convection. Given the height of the chimney, the elevated release point would enable further dispersion before reaching the ground. However, even though it may cool the fuel sufficiently, it is unclear whether such a system would be satisfactory from public health and social acceptance perspectives.

Several methods may be used that would eliminate the contact of the air with the fuel salt. First, the air may flow through tubes which pass through the drained fuel salt. This would provide the same means of cooling that is present in the previously analyzed sys-

tem. Alternatively, the natural convection cooling may be eliminated. The radiative losses would then be used to cool the drained fuel salt. Doing this, the cooling tank can be of a uniform depth, as the establishment of the natural convective flow path will not be necessary. Using a depth of 0.05 m, the maximum temperature reached is 921°C. Using initially solid salt 0.1 m in depth and increasing the fuel salt depth to 0.1 m, the maximum temperature reached is 888°C.

5.4.6 Reactor Power Limitations

Throughout this discussion, the proposed system augmentations have been analyzed for the 2250 MW MSBR reference design. The issue of the maximum power achievable with a reactor has not been addressed directly. For use in a global warming response, it is desirable to create the largest possible nuclear reactor system, using the largest possible individual power plants.

The power capacity of the augmented molten salt reactor is limited by the decay heat removal capability of the system. The volumetric decay heat load is determined by two factors: the power rating and the fuel salt volume. Altering either of these parameters will dramatically affect the fission product decay power. An increase in the reactor power rating may be achieved by either increasing the neutron flux or fissile isotope concentration in the core region or by increasing the core volume. Increasing the fuel fissile enrichment is usually unattractive economically. An increase in the neutron flux will lessen the moderating graphite life, thereby making an increase in the core volume more attractive. A core volume increase will correspond to a fuel salt volume increase. Balancing the increased reactor power rating with the fuel salt volume increase, the decay power density load may be tailored to almost any value. With an unlimited primary system volume, the power level of the system may be increased without bound.

Chapter 6

Further Work

This investigation has considered aspects of molten salt reactors which have not been considered for many years. With the halting of MSBR development efforts, technological areas which require additional examination were put aside. Several topics are of particular interest.

First, the design of the reactor core should be given more attention. Utilizing an on-line system for graphite replacement which would replace the graphite segment-by-segment, the difficulty associated with replacing the entire graphite assembly would be avoided. Further design work is required to implement such a system.

The reactor neutronics and fuel system must also be evaluated with the use of an on-line processing system. The rate of ^{232}Th makeup must be determined so that steady state operation is ensured.

It has been postulated that the processing system could have a one day effective cycle time. This value was not based upon equipment capacities or limitations. It is plausible that this value could be reduced further, thereby decreasing the period of time over which the decay heat removal system must remove a heat load comparable to solid fuel reactors.

Additional work must also be done to determine the decay heat load experienced if a processing cycle time of less than ten days is employed. The method used for the estimation of the decay power is invalid for short processing times or long operating times. Therefore, more exact methods of the determination of the concentration of fission products should be employed.

The rapid decrease of flow upon pump failure is also of concern. Experiencing a 0.89 MPa pressure loss solely in the primary heat exchanger, the molten salt circulating pump is a critical system component. A redesign of the heat exchanger would be required for buoyancy-driven natural convection circulation of the molten salt.

Finally, the cooling system for the drained fuel salt requires the use of a radiation transparent cover. This cover may be made of a material such as quartz, however it may be easily damaged and it must be kept clean in order for it to function sufficiently. The use of alternate geometries or reflectors may resolve these difficulties.

Chapter 7

Review and Conclusions

For the future of our planet, an alternate means of energy production must be developed to mitigate the effects of global warming. A nuclear system suitable for this use must be capable of large-scale power production, fuel breeding, hydrogen production, on-line fission product removal, and nuclear proliferation resistance.

The molten salt breeder reactor encompasses these required characteristics. Utilizing the ^{232}Th-^{233}U fuel cycle, breeding is achieved and a barrier to nuclear proliferation is provided inherently. Circulating a fluid fuel, the fission products may be actively removed with an on-line chemical processing system.

Development efforts to-date on molten salt breeder reactors were concentrated at the Oak Ridge National Laboratory with the design of the MSBR. Using a LiF-BeF_2 based fuel salt, NaF-$NaBF_4$ secondary coolant, and steam turbine cycle, a total system efficiency of 44% is achieved. The interactions of the fuel and coolant salts are negligible, however the contact of the steam with either of these fluids should be avoided. Use of the improved HN80MTY alloy can minimize the effects of corrosion upon the container and piping materials. By coating the moderating graphite with pyrolytics or silicon carbide, the graphite appears to be capable of four years of continuous operation without replacement.

The processing system developed by ORNL for use with the MSBR consisted of three stages. First, the fuel was fluorinated to remove the uranium. Second, a reductive extraction of the protactinium was performed. Finally, a metal transfer process removed the fission products from the fuel salt. The fluorination-reductive extraction technique was never

demonstrated in continuous operation due to the lack of continuous fluorinators. The three stages of processing were never performed sequentially on the fuel salt.

This MSBR proposed system developed at ORNL possessed three major weakness: (1) the complicated chemical processing scheme, (2) the potentially harmful interactions of steam with the salts, and (3) the lack of passive cooling systems.

The processing system could be effectively reduced to a one step, metal transfer process for the removal of fission products. Such a system could be capable of a one-day processing time with approximately a 100% efficiency. This would effectively decrease the long-term decay heat production significantly. However, for periods shorter than the processing cycle time, the decay power would be comparable to that of solid fuel reactors.

The harmful interactions of steam with the fuel and secondary coolant salts may be avoided with the use of helium based gas turbines. This inert gas will not react with either salt.

A natural circulation system may be employed to maintain flow passively in the primary circuit in the event of pump failure. With a total system height of 15 m, the flow will assume a mass flow rate which will be sufficient to avoid the overheating of the fuel.

Finally, an air-based natural convection cooling system may be employed to remove the decay heat from the fuel salt which has been drained from the primary system. With the system illustrated in Chapter 5, the temperature of the fuel salt is maintained below the point at which the fission products would volatilize. Use of this decay heat removal system would enable the reactor power to be increased without bound, provided an increase in primary system volume.

With these system augmentations, the degree of passive safety of the molten salt reactor system is enhanced. Capable of large-scale breeding, hydrogen production, active fission product removal, and resistance to nuclear proliferation, this safe reactor system

meets all of the characteristics required in a global warming mitigation effort. Thus, the molten salt breeder reactor represents a viable and sustainable energy option to ensure the long-term protection of the global environment.

Appendix A

The Oak Ridge National Laboratory Molten Salt Breeder Reactor (MSBR)

The latest design of a molten salt breeder reactor with on-line chemical processing was the MSBR developed at ORNL. Throughout the work reported here, the modified systems were applied to this design. A schematic of the plant is presented here along with pertinent system and primary heat exchanger parameters.

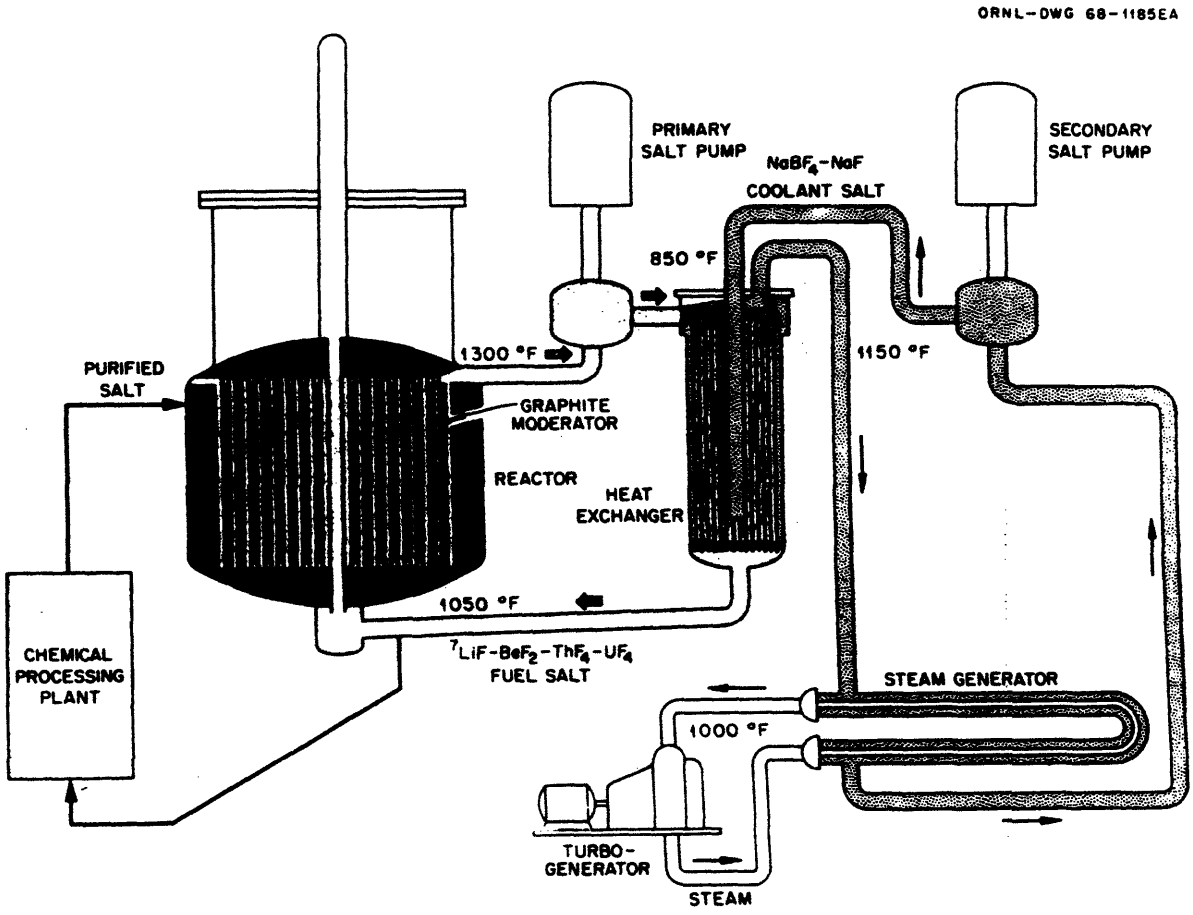

Figure A.1: A Schematic of the MSBR [36]

Table A.1: Characteristics of the 1000 MWe MSBR[36]

Useful heat generation, MWth	2250
Net electrical output of plant, MWe	1000
Overall plant thermal efficiency, %	44
Fuel salt inlet and outlet temperatures, °C	566, 704
Coolant salt inlet and outlet temperatures, °C	454, 621
Throttle steam conditions	24.13 MPa, 538°C
Reactor vessel inside diameter and height, m	6.71, 6.10
Core height, m	3.96
Core diameter, m	4.27
Radial blanket thickness, m	0.46
Graphite reflector thickness, m	0.76
Number of core elements	1412
Size of core elements, m	0.10 x 0.10 x 4.51
Salt volume fraction in core, %	13
Salt volume fraction in unmoderated region, %	37
Salt volume fraction in reflector, %	<1
Total weight of graphite in reactor, kg	669,000
Maximum salt velocity in core, m/s	2.59
Pressure drop through reactor due to flow, MPa	0.12
Average core power density, W/cm^3	22
Maximum thermal neutron flux, n/cm^2s	8.3×10^{14}
Graphite damage flux (>50 keV) at point of maximum damage, n/cm^2s	3.33×10^{14}
Estimated graphite life at maximum damage points, years	4
Total salt volume in primary system, m^3	48.70
Thorium inventory, kg	68,000
Fissile fuel inventory of reactor system and processing plant, kg	1504
Breeding ratio	1.07
Fissile fuel yield, %/year	3.6
Fuel doubling time (exponential), years	19

Table A.2: Primary Heat Exchanger Design Data [29]

	Each of 4 units
Thermal duty, MW	563.34
Tube-side conditions:	
Fluid	Fuel Salt
Entrance temperature, °C	704
Exit temperature, °C	566
Mass flow rate, kg/s	2986
Volume of salt in tubes, m^3	1.81
Number of tubes	5900
Nominal tube o.d., cm	11.40
Tube thickness, cm	0.09
Tube spacing on pitch circle, cm	1.91
Radial distance between pitch circles, cm	1.52
Length, m	6.58
Effective surface, m^2	1021.93
Pressure drop, MPa	8.89
Velocity in tubes, average m/s	3.05
Shell-side conditions:	
Fluid	Coolant Salt
Entrance temperature, °C	454
Exit temperature, °C	621
Mass flow rate, kg/s	2243
Inside diameter of shell, m	1.65
Shell thickness, cm	6.35
Baffle spacing, m	0.34
Pressure drop, MPa	0.51
Velocity, typical, m/s	2.29
Overall heat transfer coefficient, based on log mean Δt_t, tube o.d., W/m^2 °C	5394

Appendix B

Model Derivation for Natural Circulation in the Event of Pump Failure

B.1 Introduction

The ability of a system to support a natural circulation flow regime is a very powerful passive safety feature. The determination of the equilibrium flow rate achieved with the configuration described in Section 5.3 is explained here in further detail. Balancing the fuel salt buoyancy head with the friction, form, and acceleration pressure losses incurred yields the rate of change of the mass flow rate and the equilibrium value which it approaches. The details of the geometry used in this analysis are given in Figure B.1.

B.2 Conservation of Momentum

The rate of change of the primary system flow rate obeys the law of the conservation of momentum as applied to the primary loop. This rate of change is given by the following:

$$\sum_k \left(\frac{L_k}{A_k}\right)\frac{\partial}{\partial t}\dot{m} = \Delta p_{pump} - \Delta p_{friction} - \Delta p_{form} - \Delta p_{acceleration} + \Delta p_{buoyancy}. \tag{B.1}$$

In the case of pump failure, the term, Δp_{pump}, may be set equal to zero. At steady state, the mass flow rate through the primary system assumes a constant value. The remaining terms may be expanded and the differential equation solved to produce an expression for the fuel salt mass flow rate as a function of time after pump failure.

The analysis begins with the frictional pressure losses. For each uniform geometric region, the friction term may be expressed as:

$$\Delta p_{friction} = \frac{f\dot{m}^2}{2\rho DA^2}. \tag{B.2}$$

The friction factor, f, is a function of the Reynolds number of the flow. For this study, the

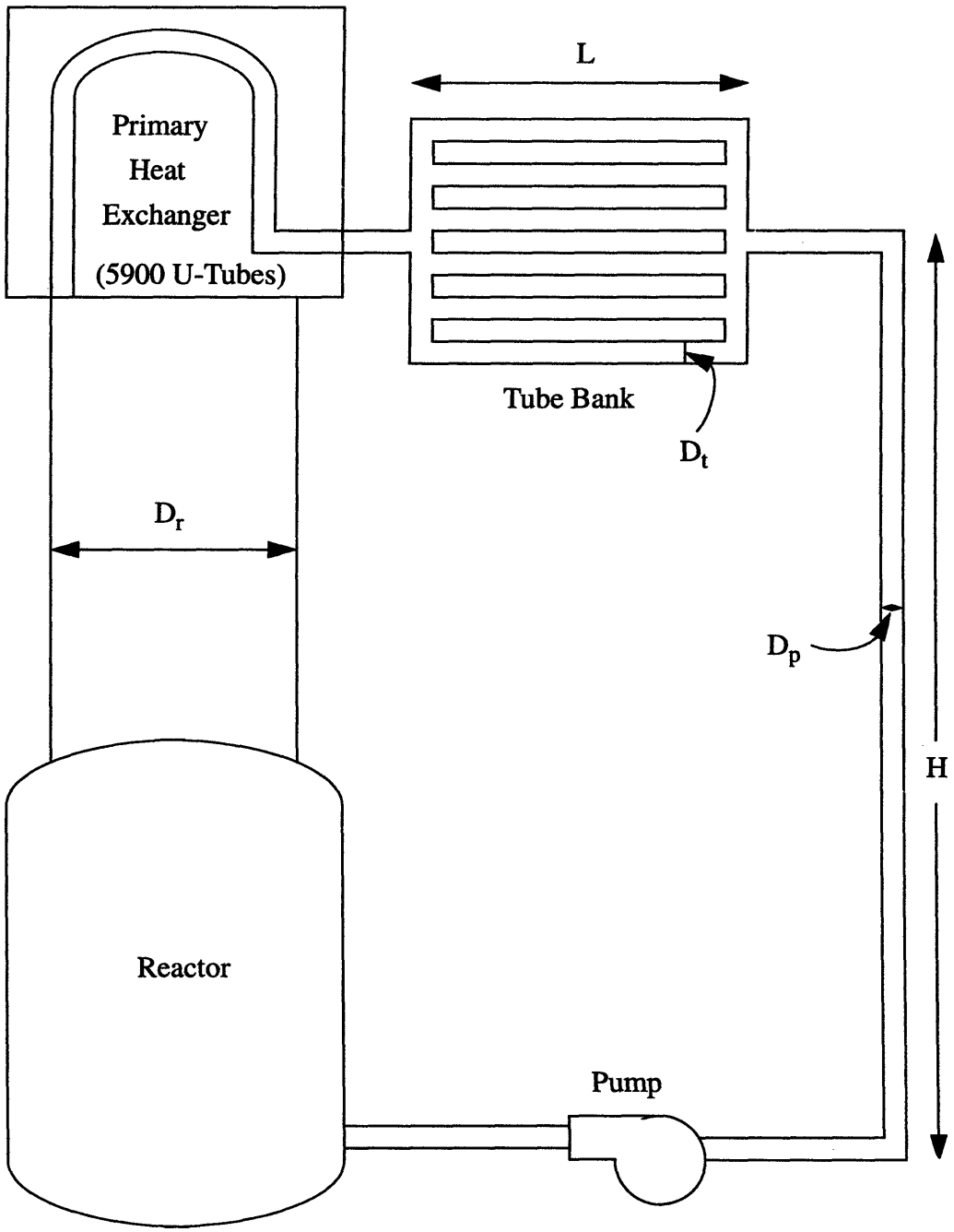

Figure B.1: Schematic Diagram of the Natural Circulation Primary System Geometry Analyzed in the Work Reported Here, Dimensions Labelled

following relations were utilized.

For laminar flow (Re < 2100):

$$f = \frac{64}{Re}, \tag{B.3}$$

In the transition region for Re < 30,000:

$$f = 0.316Re^{-0.25}, \tag{B.4}$$

For fully turbulent flow with 30,000 < Re < 1,000,000:

$$f = 0.184Re^{-0.2}. \tag{B.5}$$

Summing the frictional pressure losses throughout the entire primary circuit, the $\Delta p_{friction}$ term may be calculated [9].

Next, the form losses contribute to the overall pressure drop. In this system, these losses occur at bends and plena. Form pressure losses are given by the following empirical relation:

$$\Delta p_{form} = \frac{K\dot{m}^2}{2\rho DA^2}, \tag{B.6}$$

where K is the form loss coefficient and D is the diameter of the pipe which contains the higher velocity flow. Table B.1 summarizes the form loss coefficients of interest for the geometry under consideration. Once again, the total form pressure loss may be found by

Table B.1: Form Loss Coefficients [9]

90° bend	0.6
Entrance from a Plenum	0.5
Exit to a Plenum	1

summing all of the contributing losses as one traverses the flow circuit.

The acceleration losses are accrued when the flow experiences a change in flow area. Acceleration pressure losses are represented by the following equation:

$$\Delta p_{acceleration} = \frac{\dot{m}^2}{2\rho}\left(\frac{1}{A^2_{k+1}} - \frac{1}{A^2_k}\right). \tag{B.7}$$

The total pressure loss due to acceleration is simply the sum over each change in flow area. For a single phase fluid at constant density, the sum of the acceleration pressure changes around the flow loop is equal to zero.

Utilizing the above expressions, the total pressure drop throughout the system may be calculated. The Boussinesq approximation allows the use of a uniform density in these expressions, as the only term which requires the exact treatment of the density change is the buoyancy term. The pressure losses due to flow in the primary heat exchanger had been computed by the team at ORNL, and therefore may be included here explicitly [29].

The driving force for the flow rate in the absence of the pump is provided by the buoyancy head. This buoyancy is the result of a low density fluid at low elevations in the system and a high density fluid at higher elevations (H) in the system. The buoyancy term may be expressed as:

$$\Delta p_{buoyancy} = gH\left(\rho_{hotleg} - \rho_{coldleg}\right). \tag{B.8}$$

The hot and cold leg densities are determined by the average temperature in each leg.

Replacing the detailed expressions for their respective pressure change components in equation B.1 yields the following differential equation:

$$\sum_k \left(\frac{L_k}{A_k}\right)\frac{\partial}{\partial t}\dot{m} = gH\left(\rho_{hotleg} - \rho_{coldleg}\right) - \frac{\dot{m}^2}{2\rho}\left\{\sum_k \left(\frac{K}{DA^2} + \frac{f}{DA^2} + \left(\frac{1}{A^2_{k+1}} - \frac{1}{A^2_k}\right) + \frac{2\rho\Delta p_{HX}}{\dot{m}_0^2}\right)\right\}. \tag{B.9}$$

The relation which expresses the mass flow rate as a function of time is given by the solution of this differential equation. The solution is as follows [38]:

$$\dot{m}(t) = \frac{1}{C}\left\{\frac{\frac{1+\dot{m}_o C}{1-\dot{m}_o C}\exp\left(2C\left(\sum_k \frac{L_k}{A_k}\right)^{-1} gH(\rho_{hotleg}-\rho_{coldleg})\,t\right)-1}{\frac{1+\dot{m}_o C}{1-\dot{m}_o C}\exp\left(2C\left(\sum_k \frac{L_k}{A_k}\right)^{-1} gH(\rho_{hotleg}-\rho_{coldleg})\,t\right)+1}\right\}, \tag{B.10}$$

where C is:

$$C = \sqrt{\frac{\left(\sum_k\left(\frac{K}{DA^2}+\frac{f}{DA^2}+\left(\frac{1}{A_{k+1}^2}-\frac{1}{A_k^2}\right)+\frac{2\rho\Delta p_{HX}}{\dot{m}_0^2}\right)\right)}{2\rho gH(\rho_{hotleg}-\rho_{coldleg})}}. \tag{B.11}$$

At long times, the mass flow rate approaches the following relationship:

$$\dot{m}(\infty) = \frac{1}{C}. \tag{B.12}$$

All variables are known in these equations with the exception of the hot and cold leg densities. In order to evaluate these terms, the heat transferred to the fuel salt must be determined.

B.3 Heat Balance

Energy is imparted to the fuel salt in four ways. These are the fission process in the core, the delayed neutron precursors, the natural convection of air across the pipes of the tube bank, and the thermal radiation emitted by the tube bank piping to the surrounding environment. The power density of the core may be used to provide an estimate of the energy imparted by the fission process. The computation of the remaining contributors is not as straightforward.

First, not all of the energy from the fission process is imparted to the fuel salt while it is in the core region. Due to the circulation of the fuel, delayed neutron precursors escape as well, imparting energy to the salt. The delayed neutron fraction for ^{233}U is 0.003. These neutrons are released in regions which do not have moderation, making them subcritical. Therefore, the energy produced is solely the energy of the beta or gamma decay of the pre-

cursors. The energy emitted, E, is typically 8 MeV [35]. This energy is conveyed to the fuel as the precursors decay. Due to the similar fission product spectra of ^{233}U and ^{235}U, the delayed neutron precursors may be approximated as those for ^{235}U [34]. The precursors may be approximated by six artificial groups, each with a characteristic half life. The half life values are shown in Table B.2.

Table B.2: The Half Lives of the 6 Representative Delayed Neutron Precursor Groups [5]

Precursor Group	Half Life (seconds)
1	55
2	23
3	6.2
4	2.3
5	0.61
6	0.23

The behavior of the decay is exponential. Therefore, the probability *P(dt)* that a decay will occur in the time interval t_1 to t_2 is:

$$P = \int_{t_1}^{t_2} \lambda e^{-\lambda t} dt = e^{-\lambda t_1} - e^{-\lambda t_2} \tag{B.13}$$

Given a large number of precursors, this probability is equal to the fraction of the precursors which will decay over the interval of interest. Assuming that each precursor group contributes equally to the delayed neutron heating, the total amount of energy deposited in the fuel over the interval t_1 to t_2 is given by:

$$\dot{q}_{delayed} = 0.003 \frac{P\eta}{P_{fission}} E \sum_i \frac{(e^{-\lambda_i t_1} - e^{-\lambda_i t_2})}{6}, \tag{B.14}$$

where P is the core power level, η is the average number of neutrons emitted per neutron

absorbed in the fuel, and $P_{fission}$ is the average energy emitted per fission. The time intervals may be translated to spatial intervals using the relation that the time for an element of mass to traverse a distance L is $L\rho A$ divided by the mass flow rate.

The natural convection cooling of the pipes by the air must also be considered. The natural convection heat transfer coefficient is dependent upon the orientation of the pipes. For vertical pipes, the heat transfer coefficient for natural convection, $h_{natconv}$, is obtained as:

$$h_{natconv} = \left\{ \frac{k_{air}}{L} \left(0.825 + \frac{0.387\,(Ra_L)^{\frac{1}{6}}}{\left[1 + \left(\frac{0.492}{Pr} \right)^{\frac{9}{16}} \right]^{\frac{8}{27}}} \right) \right\}^2, \tag{B.15}$$

where Ra_L is:

$$Ra_L = \frac{2g\,(T - T_\infty)\,L^3}{\nu\alpha\,(T + T_\infty)}. \tag{B.16}$$

Pr is the Prandtl number of the air, ν is the kinematic viscosity, and α is the thermal diffusivity. For horizontal pipes, h is given by the relationship:

$$h = \frac{k_{air}}{D} C Ra_D^N, \tag{B.17}$$

where Ra_D is:

$$Ra_L = \frac{2g\,(T - T_\infty)\,D^3}{\nu\alpha\,(T + T_\infty)} \tag{B.18}$$

The values of C and N are given by Incropera and DeWitt [39]. The overall heat transfer coefficient, U, includes not only the natural convection on the external surface of the pipes, but also the convective heat transfer to the pipe from the fuel salt and the conduction through the pipe. The overall heat transfer coefficient is given by the relationship:

$$U = \frac{1}{\frac{1}{h_{natconv}} + \frac{\delta}{k_{pipe}} + \frac{1}{h_{fuel}}}, \tag{B.19}$$

where δ is the pipe thickness and h_{fuel} is given by:

$$h_{fuel} = \frac{k_{fuel}}{D} 0.023 Re^{0.8} Pr^{0.4}. \tag{B.20}$$

Once the heat transfer coefficient has been determined, the heat transfer rate may be computed according to:

$$\dot{Q}_{conv} = UA_s (T - T_\infty), \tag{B.21}$$

where A_s is the surface area of the pipe.

The radiative energy losses to the surroundings are the final component to be considered. Assuming that the pipe behaves approximately as a blackbody and is not insulated, the losses may be approximated as [39]:

$$\dot{Q}_{rad} = A_s \sigma (T^4 - T_\infty^4). \tag{B.22}$$

Knowledge of the heat imparted by the fission process, delayed neutrons, natural convection, and radiation enables the determination of the fuel salt density change. The following relationship yields the temperature change of the salt:

$$\dot{Q} = \dot{m} c_p (T_{final} - T_{initial}). \tag{B.23}$$

These temperatures may be translated to the fluid densities by the following relationship:

$$\rho_{final} = \rho_{initial} (1 - \beta (T_{final} - T_{initial})). \tag{B.24}$$

where β is the expansivity of the fuel salt. For molten salts, the expansivity is typically on the order of 5×10^{-4}/K [40].

Using the above method, the densities of the fuel salt may be determined for both the hot and cold legs of the primary loop. These values can then be substituted into the equa-

tion for the mass flow rate. With all parameters in the mass flow rate function known, the behavior of the mass flow rate may now be computed over time.

Appendix C

Model Derivation for the Natural Convection Cooling of the Drained Fuel Salt

C.1 Introduction

The purpose of this appendix is to develop the model used for the calculation of the cooling capacity of the natural convection cooling system. The determination of the heat rejection capabilities of the system described in Section 5.4 may be accomplished in two steps. The first step consists of the calculation of the mass flow rate of air induced by the buoyancy head. The computation of the heat rejected and the resultant temperature profile through the fuel salt depth is completed in the second step. Repeating this process over sequential time intervals yields the temperature profile through the salt as a function of time.

C.2 Air Mass Flow Rate

The geometry of the system is shown in Figure C.1. The height, dimensions of the salt tank, depth of the salt, and width of the duct above the fuel may be varied to achieve the optimal conditions for maximum heat transfer. The air mass flow rate plays a significant role in the heat transfer as it cools the fuel by convection.

The analysis is begun with a mass balance. This is done as follows:

$$\dot{Q}_{12} = \dot{m} c_{p,air} (T_2 - T_1) = h A_h (T_{fuel} - T_{avg}) \ , \qquad \text{(C.1)}$$

where A_h is the surface area of the fuel. The heat transfer coefficient, h, may be given by the relation for circular tubes, using the appropriate hydraulic diameter [41]. For the turbulent conditions experienced in this model, h is given by:

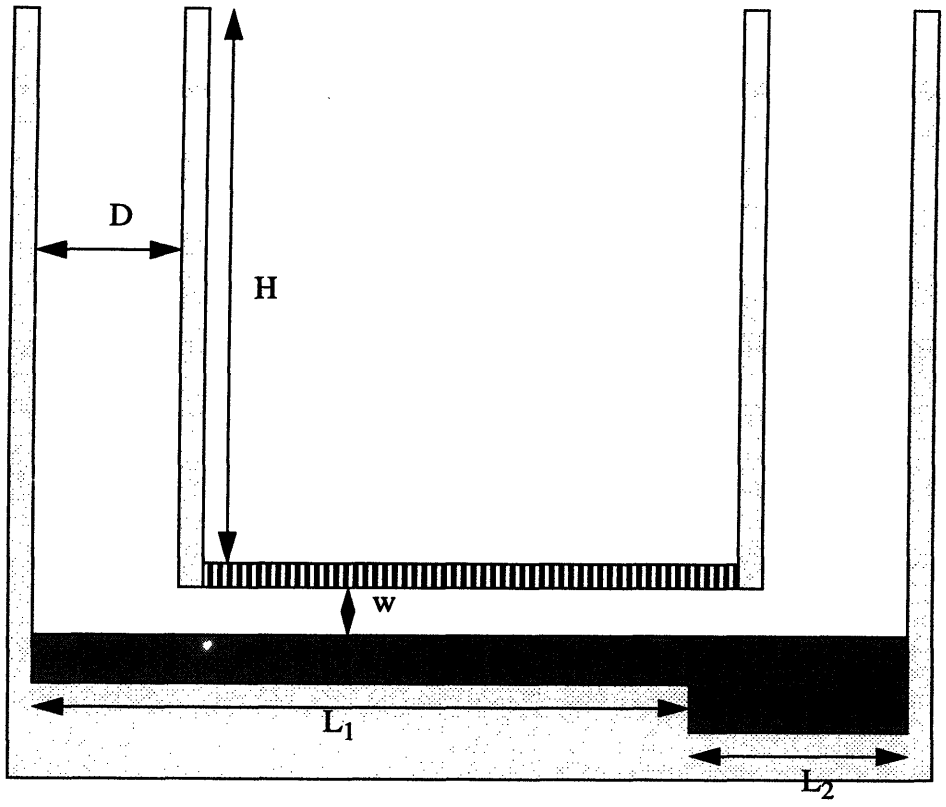

Figure C.1: Schematic Diagram of the Geometry of the Natural Convection Cooling Tanks Analyzed in the Work Reported Here, Dimensions Labelled

$$h = \frac{k}{D_h} 0.023 Re^{0.8} Pr^{0.4}. \tag{C.2}$$

The average temperature of the air is simply the average of the inlet and outlet temperatures over the interval under consideration. For the outlet temperature over the interval, algebraic manipulation yields the following relationship:

$$T_2 = \frac{\dot{m} c_{p,air} T_1 + hA_h \left(T_{fuel} - \frac{T_1}{2} \right)}{\dot{m} c_{p,air} + \frac{1}{2} hA_h}. \tag{C.3}$$

With this relationship for the temperature increase of the air, a force balance may be performed. The forces acting upon the air are those of buoyancy and momentum loss. First, the buoyancy head may be expressed as:

$$\Delta p_B = g(\rho_{in} - \rho_{out})H. \tag{C.4}$$

In this term, knowledge of the densities of the air at the inlet and outlet is required. Assuming ideal gas behavior for the air, the densities are simply a function of the temperature. These temperatures are found according to equation (C.3).

The momentum loss term includes both the friction due to flow through the ducts and the form losses at the corners. Once again, the circular tube correlations may be employed with the hydraulic diameter to determine the friction factors, f, for each flow region [41]. This relation is the following:

$$f = 0.079Re^{-0.25}. \tag{C.5}$$

The form loss coefficients, K, for sharp 90° bends are a function of the distance between the bends and the dimensions of the ducts. For the geometry under consideration, the appropriate K value is approximately 1.575 [42]. This yields the following expression for the momentum pressure loss:

$$\Delta p_F = \dot{m}^2\left(\frac{f_{in}H}{2D\rho A_{in}^2} + \frac{f_{L_1}L_1}{2w\rho A_{L_1}^2} + \frac{f_{L_2}L_2}{2w\rho A_{L_2}^2} + \frac{f_{out}H}{2D\rho A_{out}^2} + \frac{K}{2\rho A_{L_1}^2} + \frac{K}{2\rho A_{L_2}^2}\right). \tag{C.6}$$

The areas in this equation are the cross-sectional areas of the flow. Under the Boussinesq approximation, the change in fluid density may be considered only in the buoyancy term. The values of the density in the momentum loss term may be set equal to the inlet density.

The solution of the mass flow rate is obtained by equating the buoyancy pressure gain to the momentum pressure loss. This may only be done given the inlet and outlet temperatures of the air. The temperature increase of the air may be accurately calculated by apply-

ing the mass balance condition incrementally over the length of the duct, taking into consideration the change in depth of the salt. Determination of the temperature requires knowledge of the mass flow rate. Therefore, the solution of the resultant air mass flow rate is found iteratively.

C.3 Fuel Temperature

Once the air mass flow rate is determined, the cooling capacity of the geometry is known for that moment in time. The natural convection cools only the surface of the fuel salt. Due to the low expansivity of molten salt, the density gradient through the salt may be inadequate to produce internal mixing. For this reason, the salt may be viewed as a solid conductively-determined with a temperature profile through its depth.

The temperature gradient through the fuel salt is complicated by the uniform internal decay heat generation and the surface cooling by radiative and convective heat transfer. A numerical method which is well suited to handle this complexity is the finite difference implicit method [39]. First, the depth of the fuel salt is broken into nodes as illustrated in Figure C.2. A heat balance may then be applied to each node. For instance, the heat balance of the first node is given by:

$$q_{conv}'' + \frac{k}{\Delta x}(T_2^{p+1} - T_1^{p+1}) - q_{rad}'' + \dot{q}_{decay}\frac{\Delta x}{2} = \rho\frac{\Delta x}{2}c_{p,fuel}\frac{(T_1^{p+1} - T_1^{p})}{\Delta t} \quad . \qquad \text{(C.7)}$$

The superscript denotes the time at which the temperature is evaluated. For instance, T^p is evaluated at the end of the previous time interval, T^{p+1} at the end of the current interval. The subscript denotes the spatial node. The quantity, Δx, is the distance between the nodes with the point of the node representing the central point of the interval. For the surface nodes, the distance is therefore half that of an interior node. The convective heat transfer rate is governed by the relationship:

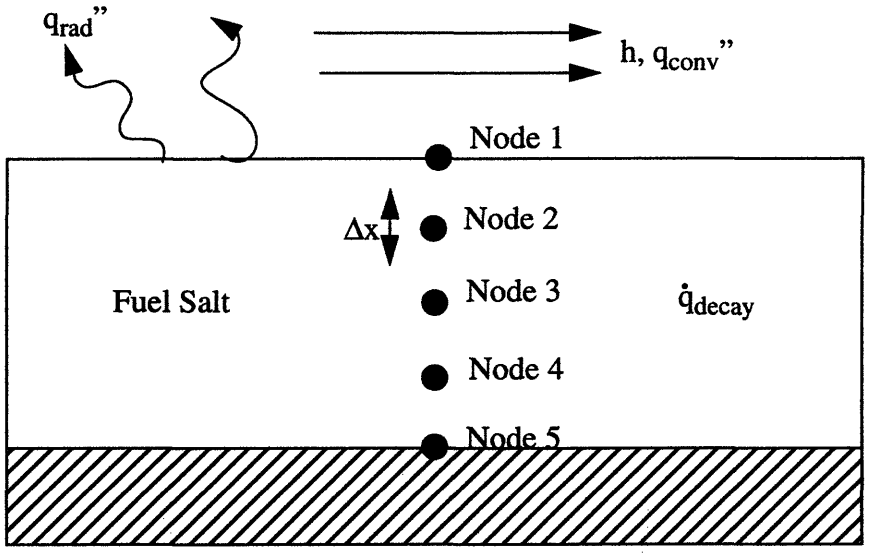

Figure C.2: The Nodal Breakdown of the Fuel Salt

$$q_{conv}'' = h\,(T_1^{p+1} - T_\infty)\,, \tag{C.8}$$

where q_{conv}" is the volumetric convective energy and h is the convective heat transfer coefficient. The radiative heat transfer may be approximated by the relationship:

$$q_{rad}'' = \sigma\tau\,(\,(T_1^{p+1})^4 - T_\infty^4)\,, \tag{C.9}$$

where τ is a measure of the transparency of the cover. This assumes that the fuel may be estimated as a blackbody [39].

Special attention must be given to node 5 which is located at an adiabatic boundary. In order to simulate this condition, node 5 may be treated as an interior node neighbored on each side by node 4. This is the condition of symmetry which is also adiabatic [39]. Using this approach, the heat balance at node 5 is given by the relationship:

$$\frac{k}{\Delta x}(T_4^{p+1} - T_5^{p+1}) + \frac{k}{\Delta x}(T_4^{p+1} - T_5^{p+1}) + \dot{q}_{decay}\Delta x = \rho\Delta x c_{p,fuel}\frac{(T_5^{p+1} - T_5^{p})}{\Delta t}, \tag{C.10}$$

or

$$\frac{k}{\Delta x}(T_4^{p+1} - T_5^{p+1}) + \dot{q}_{decay}\frac{\Delta x}{2} = \rho\frac{\Delta x}{2}c_{p,fuel}\frac{(T_5^{p+1} - T_5^{p})}{\Delta t}. \tag{C.11}$$

Forming the heat balance equations for all nodes, the following system of equations results:

$$\begin{bmatrix} 1+2F_o+2F_oB_i & -2F_o & 0 & 0 & 0 \\ -F_o & 1+2F_o & -F_o & 0 & 0 \\ 0 & -F_o & 1+2F_o & -F_o & 0 \\ 0 & 0 & -F_o & 1+2F_o & -F_o \\ 0 & 0 & 0 & -2F_o & 1+2F_o \end{bmatrix} \begin{bmatrix} T_1^{p+1} \\ T_2^{p+1} \\ T_3^{p+1} \\ T_4^{p+1} \\ T_5^{p+1} \end{bmatrix} = \begin{bmatrix} 2F_oB_iT_\infty + \frac{F_o\Delta x}{k}(-2q_{rad}'' + \dot{q}_{decay}\Delta x) + T_1^p \\ \frac{F_o(\Delta x)^2}{k}\dot{q}_{decay} + T_2^p \\ \frac{F_o(\Delta x)^2}{k}\dot{q}_{decay} + T_3^p \\ \frac{F_o(\Delta x)^2}{k}\dot{q}_{decay} + T_4^p \\ \frac{F_o(\Delta x)^2}{k}\dot{q}_{decay} + T_5^p \end{bmatrix}, \tag{C.12}$$

where

$$F_o = \frac{\alpha\Delta t}{(\Delta x)^2}, \tag{C.13}$$

and

$$B_i = \frac{h\Delta x}{k}. \tag{C.14}$$

This matrix relationship may be written more simply as [A][T]=[C]. Using the inverse matrix $[A^{-1}]$, the temperatures at the current interval may be calculated as $[T]=[A^{-1}][C]$. Because the radiative heat loss is a function of T_1^{p+1}, the solution must be determined iteratively [39]. The temperature profiles through each of the salt regions may be computed independently.

This method calculates the temperature change over a discrete interval. Due to the implicit nature of the calculation, there is no stability restriction on the length of the inter-

val. Repeating the process, the temperature profile through the sait depth is determined throughout time.

Appendix D

Use of Initially Solid Salt in the Natural Convection Cooling of the Drained Fuel Salt

D.1 Introduction

The natural convection cooling system analyzed in Appendix C may be augmented with the addition of initially solid non-fissile salt in the base of the cooling tanks. Doing this provides a heat sink which decreases the decay power burden at short times after the fuel is drained. The model developed in Appendix C must be modified to handle the melting of the solid salt. This modification is described here.

D.2 The Salt Temperature

As the initially solid salt is heated and then begins to melt, the heat of the fuel salt is distributed over the solid salt. In order for the salt to melt, an amount of energy equal to the product of the salt mass and the heat of fusion of the salt must be consumed. Figure D.1 illustrates the nodal breakdown of the fuel and non-fissile salts. In the initially solid salt region, the heat balance is given by the following relationship:

$$\frac{k}{\Delta x}(T_5^{p+1} - T_6^{p+1}) + \frac{k}{\Delta x}(T_7^{p+1} - T_6^{p+1}) + \frac{q_{HF}}{\Delta t}\Delta x = \rho \Delta x c_{p,fuel}\frac{(T_6^{p+1} - T_6^{p})}{\Delta t}, \qquad \text{(D.1)}$$

where q_{HF} is the heat of fusion. The value of the heat of fusion is set equal to zero when the salt is not at the melting temperature. When the melting temperature is reached, the value of q_{HF} over the interval under consideration is set equal to the amount of energy which will result in no temperature change in the node. This is done until the total q_{HF} over all intervals is equal to 3.36 x 10^9 J/m^3, at which point the node is liquefied completely [40]. For the node at the interface, the heat balance becomes,

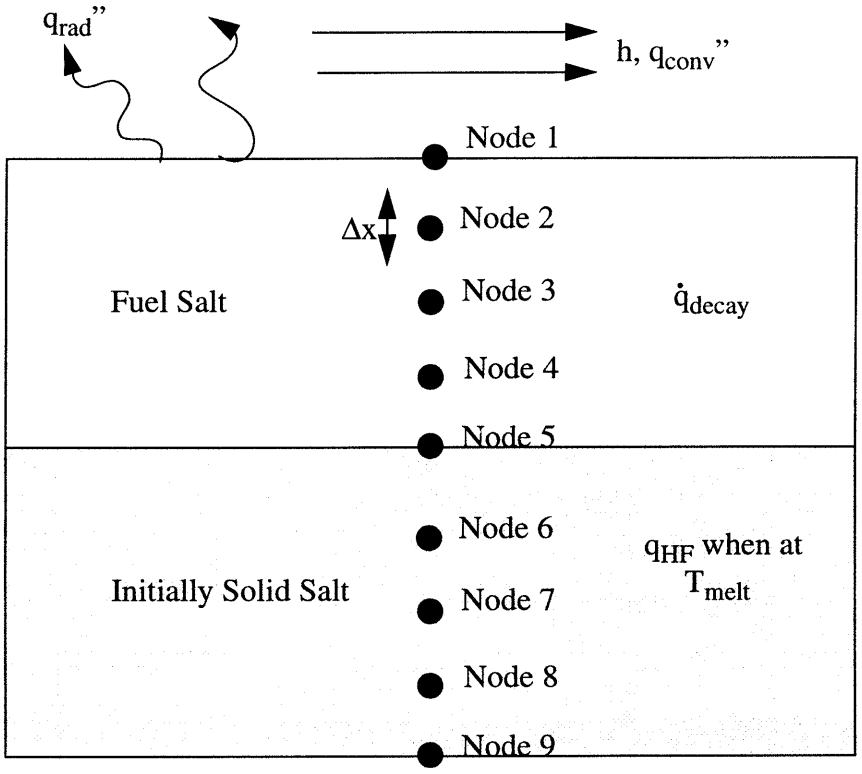

Figure D.1: Nodal Breakdown of the Fuel Salt and Initially Solid Salt

$$\frac{k}{\Delta x}(T_4^{p+1} - T_5^{p+1}) + \frac{k}{\Delta x}(T_6^{p+1} - T_5^{p+1}) + \dot{q}_{decay}\frac{\Delta x}{2} + \frac{q_{HF}}{\Delta t}\frac{\Delta x}{2} = \rho \Delta x c_{p,fuel}\frac{(T_5^{p+1} - T_5^{p})}{\Delta t} \quad \text{(D.2)}$$

A system of equations similar to that in Appendix C may be developed, where [A] becomes:

$$\begin{bmatrix} 1+2F_o+2F_oB_i & -2F_o & 0 & 0 & 0 & 0 & 0 & 0 & 0 \\ -F_o & 1+2F_o & -F_o & 0 & 0 & 0 & 0 & 0 & 0 \\ 0 & -F_o & 1+2F_o & -F_o & 0 & 0 & 0 & 0 & 0 \\ 0 & 0 & -F_o & 1+2F_o & -F_o & 0 & 0 & 0 & 0 \\ 0 & 0 & 0 & -F_o & 1+2F_o & -F_o & 0 & 0 & 0 \\ 0 & 0 & 0 & 0 & -F_o & 1+2F_o & -F_o & 0 & 0 \\ 0 & 0 & 0 & 0 & 0 & -F_o & 1+2F_o & -F_o & 0 \\ 0 & 0 & 0 & 0 & 0 & 0 & -F_o & 1+2F_o & -F_o \\ 0 & 0 & 0 & 0 & 0 & 0 & 0 & -2F_o & 1+2F_o \end{bmatrix}, \tag{D.3}$$

and [C] becomes:

$$\begin{bmatrix} 2F_oB_iT_\infty + \frac{F_o\Delta x}{k}(-2q_{rad}'' + \dot{q}_{decay}\Delta x) + T_1^p \\ \frac{F_o(\Delta x)^2}{k}\dot{q}_{decay} + T_2^p \\ \frac{F_o(\Delta x)^2}{k}\dot{q}_{decay} + T_3^p \\ \frac{F_o(\Delta x)^2}{k}\dot{q}_{decay} + T_4^p \\ \frac{F_o(\Delta x)^2}{2k}\left(\dot{q}_{decay} + \frac{q_{HF}}{\Delta t}\right) + T_5^p \\ \frac{F_o(\Delta x)^2}{k\Delta t}q_{HF} + T_6^p \\ \frac{F_o(\Delta x)^2}{k\Delta t}q_{HF} + T_7^p \\ \frac{F_o(\Delta x)^2}{k\Delta t}q_{HF} + T_8^p \\ \frac{F_o(\Delta x)^2}{k\Delta t}q_{HF} + T_9^p \end{bmatrix}. \tag{D.4}$$

Using these modified matrices, the temperature profile through the salt depth may be calculated as in Appendix C.

Appendix E

Nomenclature

The purpose of this appendix is to define the nomenclature used throughout the work reported here.

Table E.1: Nomenclature

Symbol	Definition
A	cross-sectional area, positive function of temperature for the calculation of graphite volumetric expansion
A_h, A_s	surface area
A_x	atomic mass of x
a	parameter of the gamma or incomplete gamma function
B	positive function of temperature for the calculation of graphite volumetric expansion
B_i	Biot number
b	parameter of the incomplete gamma function
C	constant
C_D	coefficient of drag
c_p	specific heat
D	drag force, distribution coefficient, diameter
D_h	hydraulic diameter
E	energy emitted per delayed neutron precursor decay
F	isotope production rate
F_o	Fourier number
f	friction factor
g	gravitational constant
H	height
h	convective heat transfer coefficient
K	form loss coefficient

Table E.1: Nomenclature

Symbol	Definition
k	thermal conductivity
L	length
$\dot{m}$	mass flow rate
$\dot{m}_o$	rated mass flow rate
N	number of atoms
P	power, decay power
P_o	steady state power
$P_{fission}$	energy emitted per fission
P_{proc}	decay power with chemical processing
$P(dt)$	probability of delayed neutron precursor decay in time interval dt
Pr	Prandtl number
$\dot{Q}$	rate of energy transfer
q	heat generation per unit volume
$\dot{q}$	rate of heat generation per unit volume
$q"$	heat flux
R_x	range in medium, x
Ra	Raleigh number
Re	Reynolds number
T	operating time, temperature
t	time
t_o	time of steady state operation
U	overall heat transfer coefficient
v	fluid velocity, volumetric expansion
w	width
α	thermal diffusivity
β	thermal expansivity
Γ	gamma function

Table E.1: Nomenclature

Symbol	Definition
γ	incomplete gamma function
Δp	pressure change
Δx	interval length
δ	thickness
Φ	neutron fluence
η	average number of neutrons created per neutron absorbed in the fuel
λ	decay constant
ν	kinematic viscosity
Π	effective processing cycle time
π	total processing cycle time
ρ	density
τ	time constant for flow decay, transparency to thermal radiation
ζ	efficiency of chemical processing system
Subscripts	
conv	convection
decay	fission product decay
delayed	decay of delayed neutron precursors
HX	primary heat exchanger
HF	heat of fusion
natconv	natural convection
rad	thermal radiation
Superscripts	
p	evaluated at end of previous time interval
p + 1	evaluated at end of current time interval

References

[1] Richard A. Kerr. "Scientists See Greenhouse, Semiofficially". *Science,* v. 269, p.1667, September 22, 1995.

[2] "The Battle for World Power". *The Economist*, p. 23, October 7, 1995.

[3] Michael W. Golay. *Barriers to Global Warming Mitigation.* Massachusetts Institute of Technology.

[4] L. M. Lidsky. "Nuclear Power: Levels of Safety." *Radiation Research*, v. 133, 1988.

[5] Ronald Allen Knief. *Nuclear Engineering: Theory and Technology of Commercial Nuclear Power,* second edition. Hemisphere Publishing Co., Washington, 1992.

[6] M. Venugopalan and R. A. Jones. *Chemistry of Dissociated Water Vapor and Related Systems.* John Wiley & Sons, New York, 1968.

[7] Ralph Moir. Summary of Visit to LLNL 7/22/94 by Professor Kazuo Furukawa. July 22, 1994.

[8] Donald R. Olander. *Fundamental Aspects of Nuclear Fuel Elements.* Technical Information Center, Virginia, 1976.

[9] Neil E. Todreas and Mujid S. Kazimi. *Nuclear Systems I: Thermal Hydraulic Fundamentals.* Hemisphere Publishing Co., New York, 1993.

[10] Roy Weinstein. *Nuclear Engineering Fundamentals: III Interaction of Radiation with Matter.* McGraw-Hill Book Co., New York, 1964.

[11] Otto Oldenberg and Norman C. Rasmussen. *Modern Physics for Engineers.* McGraw-Hill, Inc., New York, 1966.

[12] James A. Faye. *Introduction to Fluid Mechanics.* Draft of December 29, 1992.

[13] Kazuo Furukawa and Alfred Lecocq. *Preliminary Examination on "The Next Generation Nuclear Reactors" in Comparison with the Small Thorium Molten Salt Reactor.* Tokai University, December 23, 1988.

[14] S. A. Colgate and R. L. Aamodt. "Plasma Reactor Promises Direct Electric Power." *Nucleonics*, v. 15, pp. 50-55, August 1957.

[15] S. Baron. "Gaseous-fuel Reactor." *Nucleonics*, v. 16, no. 128, pp. 128-133, August 1958.

[16] S. E. Beall and C. E. Winters. "The Homogeneous Reactor Experiment." *Chemical Engineering Progress*, v. 50, pp. 256-263, May 1954.

[17] V. V. Ignatyev, V. M. Novikov, A. I. Surenkov, and V. I. Fedulov. *The State of the Problem on Materials as Applied to the Molten Salt Reactor: Problems and Ways of Solution*. Russian Research Centre, Kurchatov Institute, Moscow, 1993.

[18] M. W. Rosenthal, P. R. Kasten, and R. B. Briggs. "Molten Salt Reactors - History, Status, and Potential." *Nuclear Applications and Technology*, v. 8, no. 2, pp. 107 - 117, February 1970.

[19] A. M. Perry. "Reactor Physics and Fuel Cycles." *The Development Status of Molten Salt Breeder Reactors*, ORNL-4812, Oak Ridge, Tennessee, pp. 65 - 94, August 1972.

[20] Uri Gat and H. L. Dodds. "The Source Term and Waste Optimization of Molten Salt Reactors with Processing." *International Conference on Future Nuclear Systems: Emerging Fuel Cycles and Waste Disposal Options*, Seattle, WA, 1993.

[21] Paul N. Haubenreich and J. R. Engel. "Experience with the Molten Salt Reactor Experiment." *Nuclear Applications and Technology*, v. 8, no. 2, pp. 118 - 137, February 1970.

[22] W. R. Grimes. "Molten Salt Reactor Chemistry." *Nuclear Applications and Technology*, v. 8, no. 2, pp. 137 - 156, February 1970.

[23] H. E. McCoy. "Materials for Salt-Containing Vessels and Piping." *The Development Status of Molten Salt Breeder Reactors*, ORNL-4812, Oak Ridge, Tennessee, pp. 195 - 218, August 1972.

[24] W. R. Grimes, E. G. Bohlmann, A. S. Meyer, and J. M. Dale. "Fuel and Coolant Chemistry." *The Development Status of Molten Salt Breeder Reactors*, ORNL-4812, Oak Ridge, Tennessee, pp. 95- 167, August 1972.

[25] Dunlap Scott and W. P. Eatherly. "Graphite and Xenon Behavior and Their Influence on Molten Salt Reactor Design." *Nuclear Applications and Technology*, v. 8, no. 2, pp. 179 - 189, February 1970.

[26] W. P. Eatherly. "Graphite." *The Development Status of Molten Salt Breeder Reactors*, ORNL-4812, Oak Ridge, Tennessee, pp. 175 - 193, August 1972.

[27] W. P. Eatherly. "Developments of Irradiation-Resistant Graphites." Paper 9, *Oak Ridge National Laboratory Gas-Cooled Reactor and Molten-Salt Reactor: Information Meetings*, Oak Ridge, Tennessee, April 27 - May 1, 1970.

[28] Dunlap Scott, W. R. Huntley, A. G. Grindell, H. A. McLain, A. I. Krakoviak, E. S. Bettis, J. L. Crowley, and C. E. Bettis. "Reactor Components and Systems." *The Development Status of Molten Salt Breeder Reactors*, ORNL-4812, Oak Ridge, Tennessee, pp. 221 - 300, August 1972.

[29] E. S. Bettis and Roy C. Robertson. "The Design and Performance Features of a Single-Fluid Molten Salt Breeder Reactor." *Nuclear Applications and Technology*, v. 8, no. 2, pp. 190 - 207, February 1970.

[30] L. E. McNeese. "Fuel Processing." *The Development Status of Molten Salt Breeder Reactors*, ORNL-4812, Oak Ridge, Tennessee, pp. 331- 362, August 1972.

[31] M. E. Whatley, L. E. McNeese, W. L. Carter, L. M. Ferris, and E. L. Nicholson. "Engineering Development of the Molten Salt Breeder Reactor Fuel Recycle." *Nuclear Applications and Technology*, v. 8, no. 2, pp. 170 - 179, February 1970.

[32] J. R. Engel. Personal Communication, April 1996.

[33] Uri Gat. *The Ultimate Safe (U.S.) Reactor - A Concept for the Third Millennium.* Fourth International Conference on Emerging Nuclear Energy Systems, Madrid, Spain, June 30 - July 4, 1986.

[34] Emilio Segre. *Nuclei and Particles: An Introduction to Nuclear and Subnuclear Physics.* W. A. Benjamin, Inc., new York, 1964.

[35] Allen F. Henry. *Nuclear Reactor Analysis*. The MIT Press, Cambridge, MA, 1975.

[36] M. W. Rosenthal. "Design Concept of the Molten Salt Breeder Reactor." *The Development Status of Molten Salt Breeder Reactors*, ORNL-4812, Oak Ridge, Tennessee, pp. 51- 63, August 1972.

[37] L. M. Lidsky. Personal Communication, May 1996.

[38] Neil E. Todreas and Mujid S. Kazimi. *Nuclear Systems II: Elements of Thermal Hydraulic Design*. Hemisphere Publishing Co., New York, 1990.

[39] Frank P. Incropera and David P. DeWitt. *Fundamentals of Heat and Mass Transfer*, third edition. John Wiley & Sons, New York, 1990.

[40] George J. Janz. *Molten Salts Handbook.* Academic Press, New York, 1967.

[41] Warren Max Rohsenow. *Handbook of Heat Transfer.* McGraw-Hill, New York, 1973.

[42] I. E. Idelcik. *Handbook of Hydraulic Resistance*, second edition. Hemisphere Publishing Co., Washington, 1986.